MINISTRY OF NATIONAL EDUCATION

THE ANNALS OF "DUNAREA DE JOS" UNIVERSITY OF GALATI

Fascicle IX
METALLURGY AND MATERIALS SCIENCE

YEAR XXXVII (XLII)
September 2019, no. 3

ISSN 2668-4748; e-ISSN 2668-4756

2019
GALATI UNIVERSITY PRESS

EDITORIAL BOARD

THE ANNALS OF "DUNAREA DE JOS" UNIVERSITY OF GALATI
FASCICLE IX. METALLURGY AND MATERIALS SCIENCE
Nº. 3 - 2019, ISSN 2668-4748; e-ISSN 2668-4756
Volume DOI: https://doi.org/10.35219/mms.2019.3

Table of Contents

THE ANNALS OF "DUNAREA DE JOS" UNIVERSITY OF GALATI
FASCICLE IX. METALLURGY AND MATERIALS SCIENCE
Nº. 3 - 2019, ISSN 2668-4748; e-ISSN 2668-4756
Volume DOI: https://doi.org/10.35219/mms.2019.3

THE ANNALS OF "DUNAREA DE JOS" UNIVERSITY OF GALATI
FASCICLE IX. METALLURGY AND MATERIALS SCIENCE
Nº. 3 - 2019, ISSN 2668-4748; e-ISSN 2668-4756
Article DOI: https://doi.org/10.35219/mms.2019.3.01

THE INFLUENCE OF THE NUMBER OF LEVELS ON THE BEHAVIOR OF A VERTICAL AXIS WIND TURBINE WITH TWO PAIRS OF BLADES AND PERIODIC AERODINAMIC COUPLINGS

Nelu CAZACU
"Dunarea de Jos" University of Galati, Romania
e-mail: nelu.cazacu@ugal.ro

ABSTRACT

Vertical-axis wind turbines (VAWT) with 1 pair of semi-cylindrical and overlapping blades have an uneven torque. The work is based on wind tunnel experiments on experimental models that still contain a couple of auxiliary blades. The model has several levels and constructively the role of the blades changes from one level to another. The experiments in the wind tunnel confirm the important effect of the levels with changing the role of the blades until the complexity of accomplishment increases.

KEYWORDS: wind turbines, wind tunnel, wind speed

1. Introduction

The paper continues the search for practical methods to slightly increase the efficiency but reduce the disadvantages of the wind turbine Savonius (s-rotor). A thing mentioned in many works is that the wind turbine has the advantage of constructive simplicity, independence from the wind direction and high solidity. That is why it is suitable for aircraft and pumping systems. The evolutions in the field of electrotechnics and electronics make it possible to use this wind turbine also in the generation of electricity by converting it into mechanical work and then converting it into electricity. The development of low and medium power electronic converters, at affordable prices, causes this disadvantage to fall, and at the output of the inverter system a constant continuous voltage is obtained in order to charge a battery. There is still the cancellation of an important obstacle, namely, the wind behaviour at high wind speeds. There have been found some solutions such as shading, tilting or more complex transformation of the wind into a sphere or a cylinder. There would also be a final disadvantage, namely the unevenness of the torque on a rotary, which in a two-bladed wind turbine is obvious, in this case there is a danger that the wind turbine will lock in the minimum torque position and not start the rotation.

In this case the disadvantages of the turbine are highlighted, and it is the low rotational speed which makes it necessary for special generators with a large number of pole pairs or mechanical speed multiplication systems. The low rotational speed and the wind speed make the wind directly dependent on the speed of the wind, resulting in brown variations of the generated voltages.

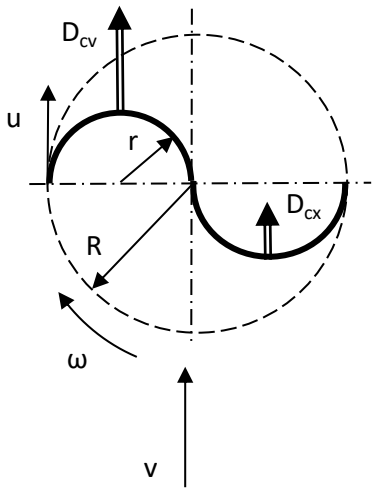

Fig. 1. *Scheme of "S-rotor" turbine with one pair of cups (1PC)* [1]

This problem is addressed in this paper to find a simple method to standardize the torque of the S-rotor wind without negatively affecting the mentioned advantages. A classic way to standardize torque is to introduce a flywheel, which is very useful when rotating at constant speed. This method brings a major disadvantage in increasing the couple when

THE ANNALS OF "DUNAREA DE JOS" UNIVERSITY OF GALATI
FASCICLE IX. METALLURGY AND MATERIALS SCIENCE
Nº. 3 - 2019, ISSN 2668-4748; e-ISSN 2668-4756
Article DOI: https://doi.org/10.35219/mms.2019.3.01

starting and accessing an existing disadvantage that is sought to be minimized.

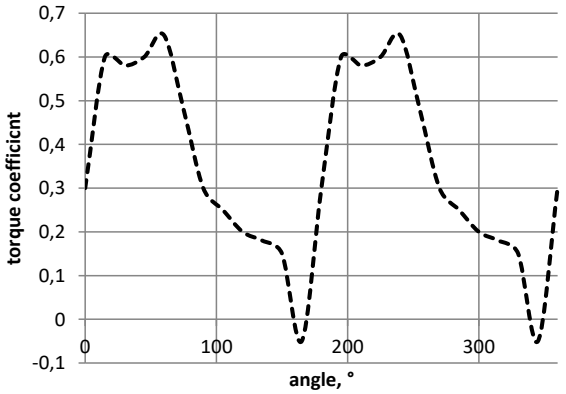

Fig. 2. *Torque for "S-rotor" (1PC) versus the rotation angle plot* [2]

In this paper we analyse the influence of multi-storey (pseudo-storey). It is considered a wind turbine Savonius with 4 semi-cylindrical cups equidistant.

Normally this structure ensures the fast and efficient starting of the S-rotor, but the load operation is defective due to the effect of the cup on the return stroke when the resistive force is high and repeated more often (at 90°).

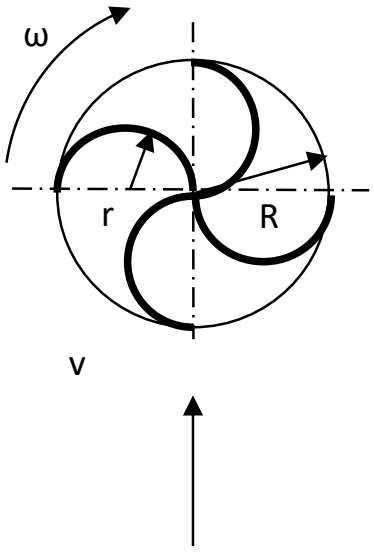

Fig. 3. *"S-rotor" with one level and two pair of cups (2PC)*

The multi-storey wind turbine with three stages offers a starting solution but does not solve the load behaviour. Each stage is offset to 120° from the previous one and, in this way, the couple is uniformized, but their starting is favoured by eliminating the dead point.

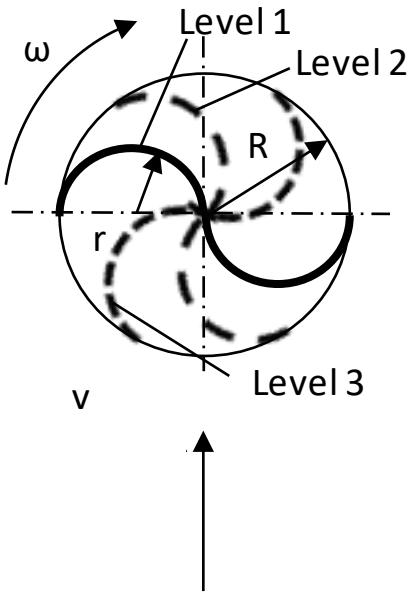

Fig. 4. *S-rotor with 3 stage and 3PC (1PC/1S)*

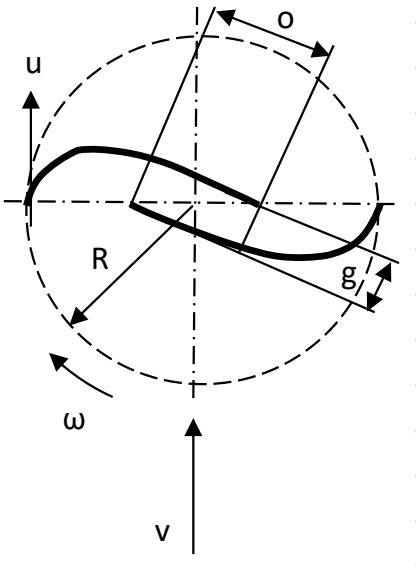

Fig. 5. *"S-rotor" of blades Benesh with gap (g) and overlay (a)* [3]

The Benesh (Fig. 2) type structure, meaning the two classic couplings no longer form an S, but the cups become separate, and thus it brings great advantages for the load-bearing operation on balance depression behind the cup at the reverse stroke on account of directing an overpressure air stream on the direct stroke

The power of wind is calculated with relation:

$$P = 0{,}5\rho A v^3 \qquad (1)$$

THE ANNALS OF "DUNAREA DE JOS" UNIVERSITY OF GALATI
FASCICLE IX. METALLURGY AND MATERIALS SCIENCE
Nº. 3 - 2019, ISSN 2668-4748; e-ISSN 2668-4756
Article DOI: https://doi.org/10.35219/mms.2019.3.01

2. Experimental conditions

The power extracted from a wind power by a VAWT "S-rotor" turbine depends on Drag force [4]:

$$D = 0{,}5C_D\rho(v-u)^2A \quad (2)$$

Where u is speed of blade and Power extracted is:

$$P = Du = 0{,}5C_D\rho v^3(1-\frac{u}{v})^2\frac{u}{v} \quad (3)$$

When:

$$\lambda = TSR = u/v \quad (4)$$

The extracted power is:

$$P = 0{,}5C_D\rho v^3(1-\lambda)^2\lambda A \quad (5)$$

And the conversion efficiency is:

$$\eta = \frac{P}{P_v} = \frac{0{,}5\rho(v-u)^2C_D uA}{0{,}5\rho Av^3} \quad (6)$$

$$\eta = \frac{(v-u)^2C_D u}{v^3} \quad (7)$$

Notations:
v - wind velocity(input), m/s
u - tip blade speed, m/s
R - the radius of the disc base, m
o - overlap, m
d - width of blade, m
h - height of blade, m
ω - angular speed, radians/s
λ - specific speed
C_p - power index
D_{cv} - drag force for concave surface
D_{cx} - drag force for convex surface

Abbreviations:
VAWT - vertical axes wind turbine
TSR - tip speed ratio
PB - pair of blades
dc - direct current
Re - Reynolds number
EM - experimental model
VCC - positive potential
GND - ground potential
EM - experimental model

3. Results

The work aims to alternate structures on an experimental model (EM) of "S-rotor" Benesh type cup structures (Fig. 2) on different floors by a simple and efficient method of periodically aerodynamically coupling the opposite blades, by overlapping and creating a pseudorandom S-rotor structure with two pairs of blades (2PB). This structure is shown in Fig. 4 and Fig. 5. In the situations presented for the loading of the experimental models, it used a multiplier (3.5x) and a 5V Dc generator.

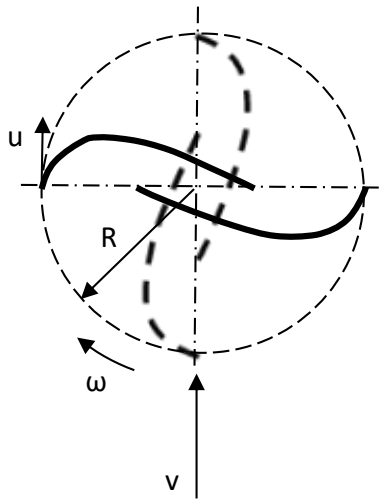

Fig. 6. *"S-rotor" with 2 level an 1PC per level in Benesh profile*

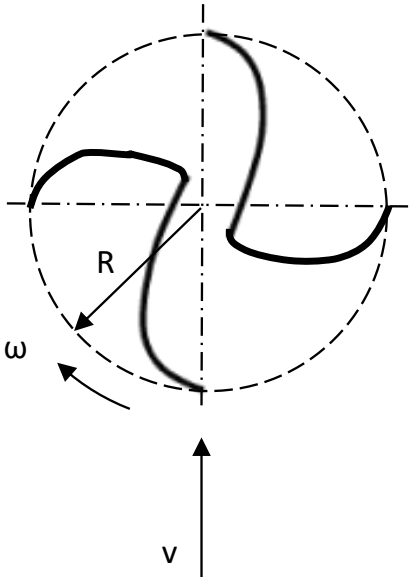

Fig. 7. *"S-rotor" through the real profile of the turbine with 2PC*

THE ANNALS OF "DUNAREA DE JOS" UNIVERSITY OF GALATI
FASCICLE IX. METALLURGY AND MATERIALS SCIENCE
Nº. 3 - 2019, ISSN 2668-4748; e-ISSN 2668-4756
Article DOI: https://doi.org/10.35219/mms.2019.3.01

The test conditions are coded as follows: N (no load mechanical or electrical), M (mechanical load multiplier x3.5 and rotor of dc generator), ML (idem M plus a white LED), ML1 (idem ML plus a 1 kΩ resistor connected VCC to GND), ML1.5 (idem ML plus a 1.5 kΩ resistor connected VCC to GND), ML2 (idem ML plus a 2 kΩ resistor connected VCC to GND).

The experiments were carried out on a wind tunnel with a wind speed between 0...4.5 m/s (measured with LCA6000).

Fig. 8-13 represents the graphs of the behaviour of the models of the experiments.

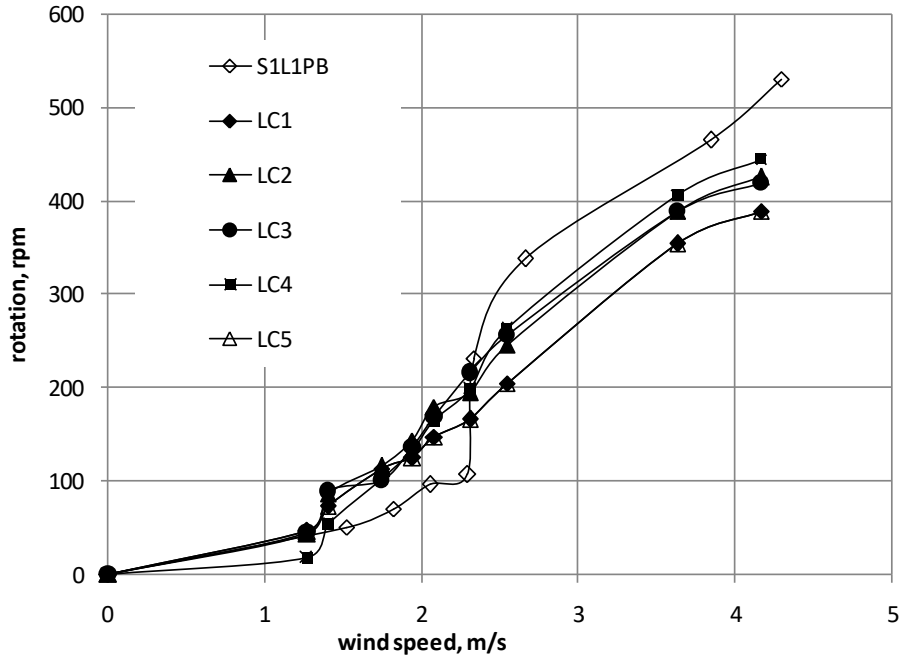

Fig. 8. *Behaviour of experimental model at N (no load)*

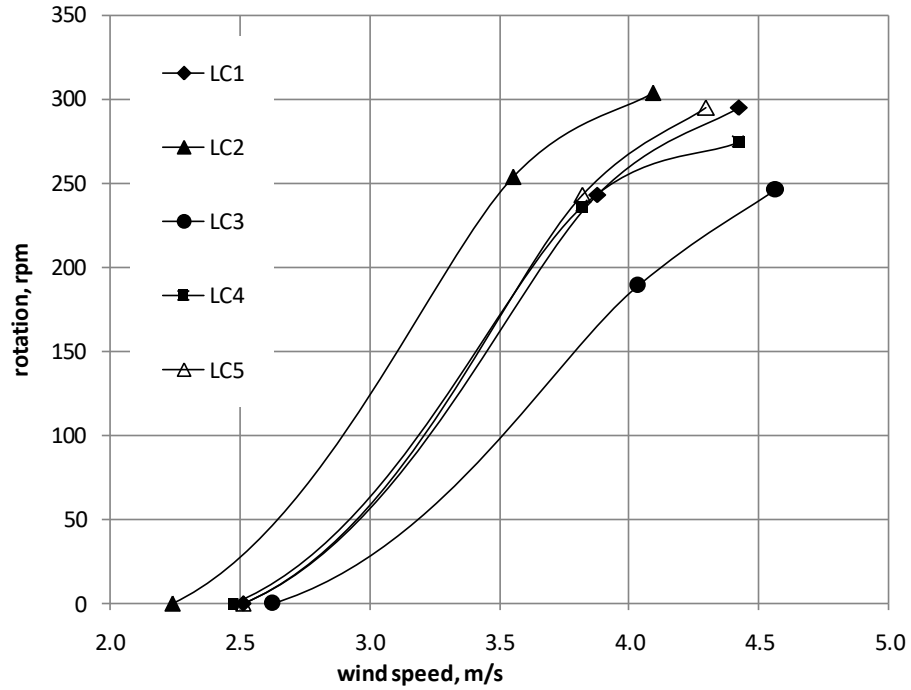

Fig. 9. *Behaviour of experimental models at load M*

THE ANNALS OF "DUNAREA DE JOS" UNIVERSITY OF GALATI
FASCICLE IX. METALLURGY AND MATERIALS SCIENCE
Nº. 3 - 2019, ISSN 2668-4748; e-ISSN 2668-4756
Article DOI: https://doi.org/10.35219/mms.2019.3.01

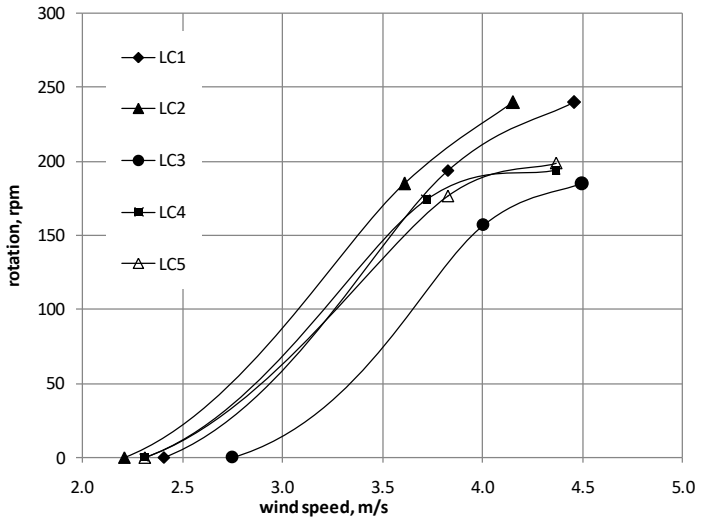

Fig. 10. *Behaviour of experimental models at load ML*

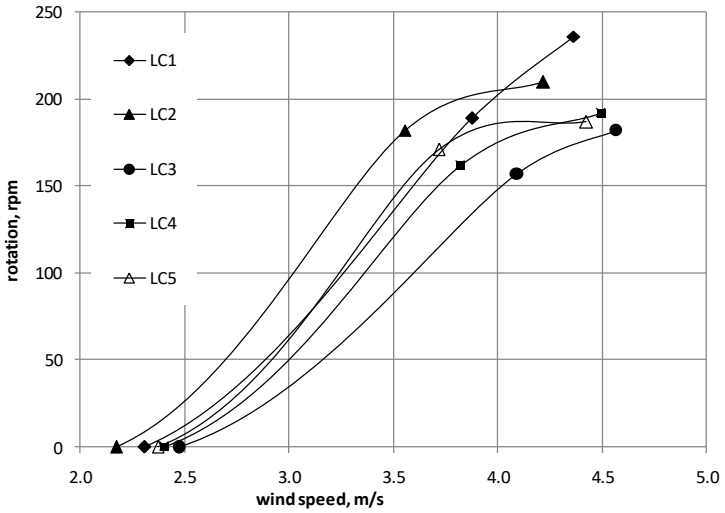

Fig. 11. *Behaviour of experimental models at load ML1*

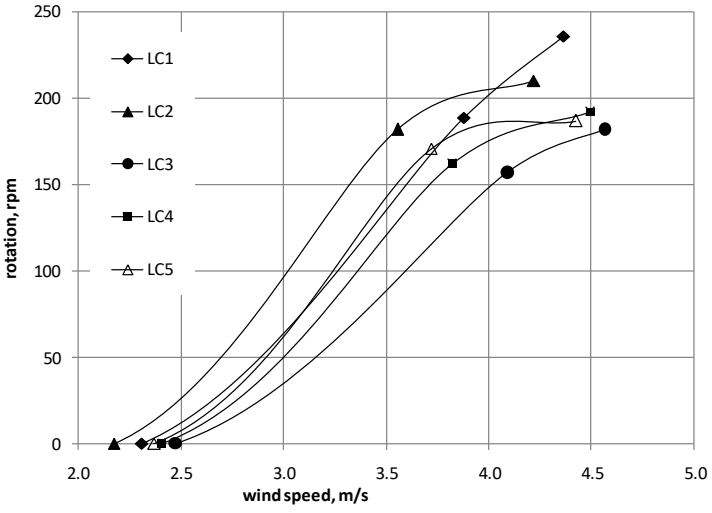

Fig. 12. *Behaviour of experimental models at load ML1.5*

THE ANNALS OF "DUNAREA DE JOS" UNIVERSITY OF GALATI
FASCICLE IX. METALLURGY AND MATERIALS SCIENCE
Nº. 3 - 2019, ISSN 2668-4748; e-ISSN 2668-4756
Article DOI: https://doi.org/10.35219/mms.2019.3.01

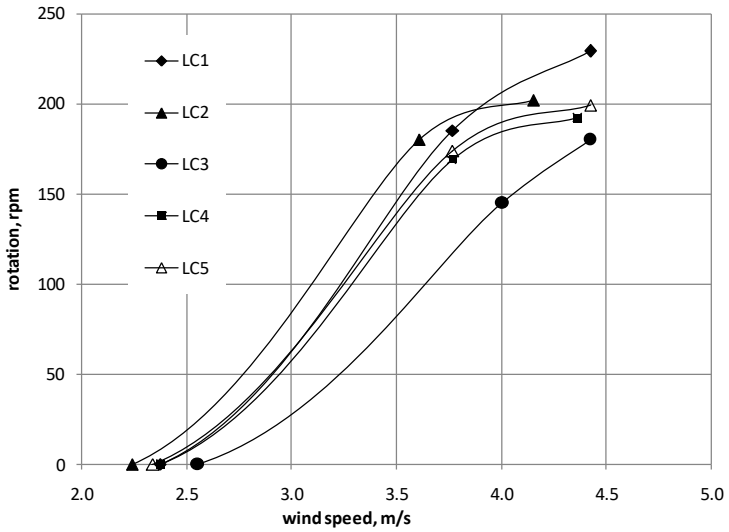

Fig. 13. *Behaviour of experimental models at load ML2*

4. Conclusions

At wind speeds less than 2 m/s, no EM starts the rotation movement. The LC2 has the best starting load.

In all experiments, the model with three equivalent levels behaved the worst with the highest starting wind speed, and at v = 4 m/s has the lowest rotations for all 5 loads.

The speed of the models is of slope and therefore with the increase of the load their speed decreases significantly. At the same speed of wind, the speed has a minimum at LC3 (Fig. 2-6) because LC2 corresponds to the lowest load resistance and therefore to the highest current. At idle (N, no load) experimental models behave very closely.

References

[1]. Hau Erich, *Wind Turbines, Fundamentals, Technologies, Applications, Economics*, s.l.: Springler, 2006.
[2]. Menet J. L., Bourabaa N., *Increase in a savonius rotor efficiency*.
[3]. Benesh A., *Wind turbine system using a vertical axis Savonius-type rotor*, US Patent 4784568, 1988.
[4]. Hansen M. L. O., *Aerodynamics of Wind Turbines*, 2nd ed., Earthscan, 2008, 2nd ed., Padstow Earthscan, 2008, ISBN: 978-1-84407-438-9.
[5]. Smulders P. T., *Rotors for wind power*, Eindhoven University of Technology, Eindhoven, Faculty of Physics, 1st edition October 1991, (revised edition January 2004).
[6]. Piggot Hugh, *Small Wind Turbine Design Notes*, 1998.
[7]. Nelson V., *Wind Energy. Renewable Energy and the Environment*, s.l.: Taylor & Francis Group LLC, 2009.
[8]. Saha U. K., Rajkumar M. J., *On the performance analysis of Savonius rotor with twisted blades*, Renewable Energy, 31, 2006.

THE ANNALS OF "DUNAREA DE JOS" UNIVERSITY OF GALATI
FASCICLE IX. METALLURGY AND MATERIALS SCIENCE
Nº. 3 - 2019, ISSN 2668-4748; e-ISSN 2668-4756
Article DOI: https://doi.org/10.35219/mms.2019.3.02

IMPROVING MECHANICAL PROPERTIES OF POLYMERIC MATERIALS USING OXIDE NANOPARTICLES

Elena Emanuela HERBEI
"Dunarea de Jos" University of Galati, Romania
e-mail: elena.valcu@ugal.ro

ABSTRACT

This paper investigated the effect of zirconium oxide (ZrO_2) and titanium oxide (TiO_2) on the morphology and mechanical properties of poly (methyl methacrylate) (PMMA) blends. Composites of PMMA (5/95 wt%) with ZrO_2 and TiO_2 were prepared by modified sol-gel reaction and then the composites were integrated by compression. The dispersion of ZrO_2 and TiO_2 nanoparticles in the polymer matrix was investigated after deposition as thin films, using optical microscope. It was studied also the transparency and the band gap of thin films of the individual compounds and of the mixed zirconia composites. It was observed that the dispersion of ZrO_2 nanoparticles was relatively good with low ZrO_2 content, but the aggregates of ZrO_2 particles in a polymer matrix increased with increasing the ZrO_2 content. The Vickers hardness test on PMMA and ZrO_2-PMMA showed that the value of hardness increases as the percentage of ZrO_2 increases. The adding of zirconia nanoparticles showed that the composites can be used in fabrication of different application as metal protection, dental materials, abrasion resistant materials, transparent protection due to the hardness tests.

KEYWORDS: zirconia nanoparticles, composites, PMMA, Vickers hardness

1. Introduction

Inorganic nanoparticles-polymeric composite has gained considerable interest due to their special properties as mechanical, thermal resistance, corrosion resistance, low density, easy processing, thermal conductivity, dielectric properties and transparency as a result of the inorganic contribution to the polymer matrix.

Polymethylmethacrylate (PMMA) is one of the most commonly used materials due to its desirable characteristics, such as excellent aesthetic properties, ease of handling and repair, accurate reproduction of surface details, lack of toxicity, and cost-effectiveness [1, 2].

When inorganic nanoparticles oxides as ZrO_2 and TiO_2 are incorporated into organic matrix, called polymer-based nanocomposites, it represents a new class of materials with improved performance compared to their mono phase counterparts [3].

In recent years, several investigations have focused on improving the mechanical properties of PMMA acrylic resins by adding functionalized nanomaterials, such as bio-ceramic nanoparticles, due to their special characteristics [4].

The functionalization agents used for these applications are organo-silica based precursors, used to improve the connection and to create new chemical bonds between the inorganic and organic compounds.

Zirconia (ZrO_2) is considered a bio-ceramic material that has been widely used for various dental applications, electronic application such as crowns and bridges, implant fixture "screws" and abutments, and orthodontic brackets [5]. Zirconia nanoparticles are used also for a high flexural strength (900 to 1200 MPa), hardness (1200 HV), and fracture toughness (9-10 MPa m1/2) [6].

Titanium oxide nanoparticles (TiO_2) is a material that has a high transparency, characterized by wide band gap and high electrical resistivity at room temperature. Also, TiO_2 is a non-toxic and exhibits good chemical, thermal and mechanical stability. In view of its properties, TiO_2 based thin films have wide range of applications. Anatase and rutile phases of tetragonal structure are the most important compounds of TiO_2 that can be used in obtaining composites using different polymer matrix for improving hardness and also for antibacterial properties [9].

Usually increased hardness of the material is strongly correlated to density of thin film. The hardness is, therefore, dependent not only on the material type, but also on its crystalline structure and crystallites size [7].

THE ANNALS OF "DUNAREA DE JOS" UNIVERSITY OF GALATI
FASCICLE IX. METALLURGY AND MATERIALS SCIENCE
Nº. 3 - 2019, ISSN 2668-4748; e-ISSN 2668-4756
Article DOI: https://doi.org/10.35219/mms.2019.3.02

The hardness of the thin films is usually many times smaller than that of the bulk. However, it was found that for thin films with dense structure the hardness is higher, and for nanomaterials it is possible to achieve the hardness even greater as compared to the bulk [8]. This is because the hardness of the material increases when the grain size decreases with the maximum in the nanometre range (Hall-Petch effect) [8]. Results of the research presented in the literature show that oxide materials, which are composed from crystallites of a single nanometres in size, exhibit completely different properties than the bulk material of the same chemical composition [10].

The purpose of this study is to evaluate the effects of zirconium oxide and titanium oxide nanoparticle addition at low concentrations (up to 10%) to a commercially available PMMA matrix on selected mechanical properties such as hardness behaviour, morphology and optical properties.

2. Experimental details

2.1. Dispersion preparation

The ZrO_2 (50 nm), TiO_2 (100 nm) nanoparticles and PMMA (495 kw) used for the preparation of dispersion were purchased from Sigma Aldrich and MICRO CHEM, respectively. For the functionalization of nanoparticles, trimetoxysilylpropyl methacrylate agent was used, in absolute ethanol as solvent, for 6 hours. After the reaction of functionalization, the nanoparticles were cleaned in isopropanol and water to eliminate the agent excess. ZrO_2-PMMA and TiO_2-PMMA dispersion with 5/95 wt% ratios were prepared (Figure 1a). Then a part of the dispersion was introduced in crucibles up to 200 ºC to eliminate the water and alcohol traces (Figure 1b).

The schematic representation of the dispersion preparation is presented in Figure 2.

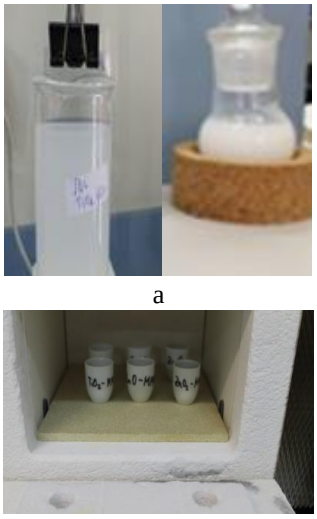

a

b

Fig. 1. *The ZrO_2-PMMA and TiO_2-PMMA resulted dispersion obtained by sol-gel modified reaction (a) and the thermal treatment of dispersion (b)*

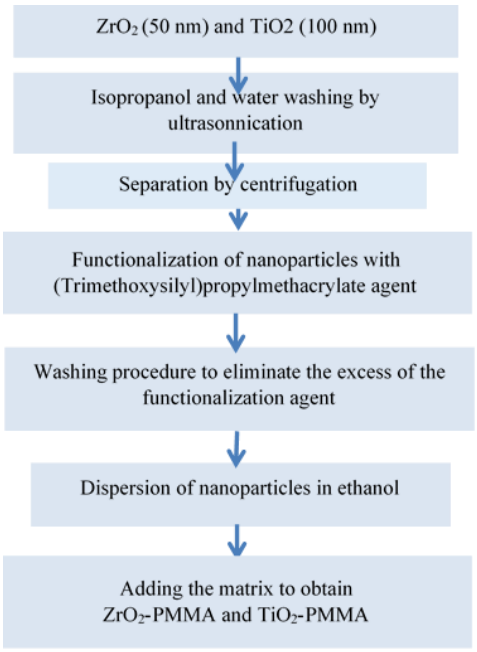

Fig. 2. *Schematic representation of modified sol-gel procedure for obtaining ZrO_2-PMMA and TiO_2-PMMA dispersion*

THE ANNALS OF "DUNAREA DE JOS" UNIVERSITY OF GALATI
FASCICLE IX. METALLURGY AND MATERIALS SCIENCE
Nº. 3 - 2019, ISSN 2668-4748; e-ISSN 2668-4756
Article DOI: https://doi.org/10.35219/mms.2019.3.02

2.2. Thin films fabrication

The glass substrates for deposition were cleaned with a standard procedure: washed in water for three times, dipping in isopropanol for 1 minute and cleaning with water, dried with nitrogen stream and heated on hotplate for 5 minutes at 120 ºC. For film preparation, the glass substrates were dip coated in ZrO_2-PMMA and TiO_2-PMMA dispersion for 20 seconds in air atmosphere, with controlled speed. The films were thermally treated on hot plate at 120 ºC for 30 minutes after they have been cleaned on the back side with alcohol.

3. Results and discussion

Results of optical microscopy investigations revealed that the thin films prepared by dip-coating process were smooth and their surface consisted of visible grains (Fig. 3).

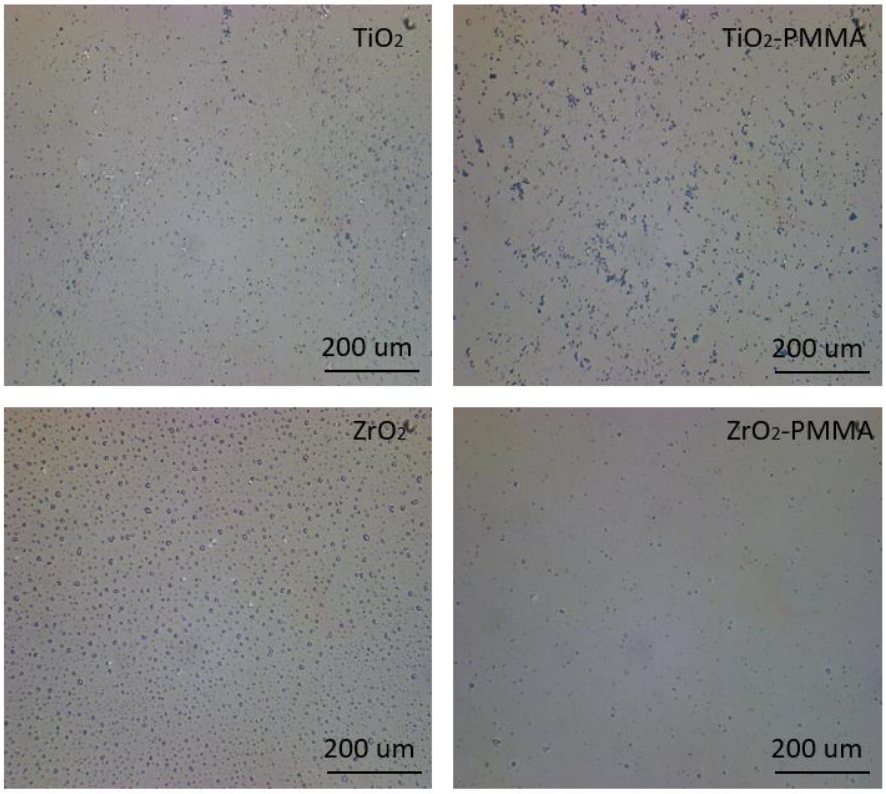

Fig. 3. *Optical microscopy for thin films*

Optical microscopy images of thin films obtained showed the agglomeration of TiO_2 and ZrO_2 nanoparticles. The embedded nanoparticles in polymer matrix showed a homogenous layer for zirconia oxide nanoparticles than titanium oxide nanoparticles. This is due probable to the electrostatic forces that appears between the TiO_2 nanoparticles.

The optical properties of zirconia oxide nanoparticles thin films show a good transparency of 91% for PMMA thin films which decrease to 85% for thin film of ZrO_2-PMMA. The sample containing TiO_2 shows a value of 80% in transparency, due to the size of nanoparticles which is 100 nm, and due to the agglomeration of nanoparticles created by the electrostatic forces. The optical transmittance of thin films obtained are presented in Figure 4.

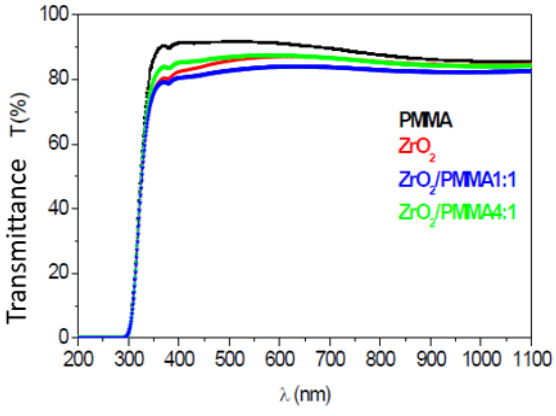

Fig. 4. *Optical transmittance for ZrO_2 and ZrO_2-PMMA thin films*

THE ANNALS OF "DUNAREA DE JOS" UNIVERSITY OF GALATI
FASCICLE IX. METALLURGY AND MATERIALS SCIENCE
N°. 3 - 2019, ISSN 2668-4748; e-ISSN 2668-4756
Article DOI: https://doi.org/10.35219/mms.2019.3.02

Micro Vickers hardness reflects the uniformity of reinforcement dispersion in composites and effect of cross-linking density on micro-level. Micro Vickers hardness values for PMMA matrix and ZrO_2-PMMA composites presented in the Figure 5 a and b. Vickers hardness number of the surface was calculated using the following formula: HV = 1.8544 F/d^2, where F is the load applied by the indenter and d is the mean diameter of the engraved diamond-shaped indent.

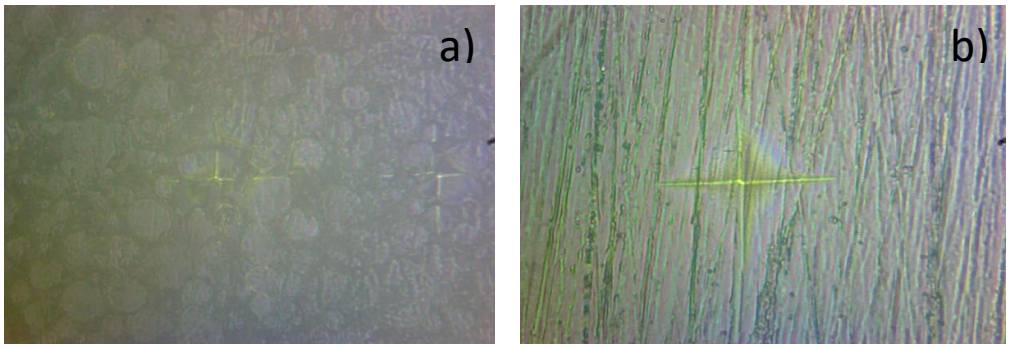

Fig. 5. *Micro-hardness test for PMMA (a) and ZrO2-PMMA (b)*

An addition of zirconia nanoparticles improved micro hardness by 40% of PMMA sample due to the uniformity of the nanoparticles in the polymer matrix and to the good dispersion of nano-ZrO_2. The improvement of the hardness is due probably to the nano size particles which helps in filling the matrix interstitially. Also, the strong adhesion formed between the functionalization agent on the surface of the nano-ZrO_2 and PMMA matrix improves the mechanical properties of nanocomposites [11, 12]. The values of Vickers hardness are presented in Table 1.

Table 1. *Micro Vickers Hardness*

Compounds	Diag. med [mm]	F (kgf)	HV 0.02/30 [kg/mm^2]	HV med
PMMA	0.044842495	0.02	18.44494211	**19.07212**
	0.04489842	0.02	18.39902108	
	0.04386418	0.02	19.27688264	
	0.04288455	0.02	20.16763708	
ZrO_2-PMMA	0.025765125	0.02	55.8717566	**41.62146**
	0.031756295	0.02	36.77876806	
	0.030916775	0.02	38.80328224	
	0.032538365	0.02	35.03203614	

4. Conclusion

Surface functionalization of nano ZrO_2 and TiO_2 was performed by using silane coupling agents with methacryloxy organo-functional groups, and after that nanoparticles was embedded in PMMA matrix. Three-layer polymer-nanoparticle oxide films with thicknesses less than 1 μm were deposed and obtained.

ZrO_2 and TiO_2 oxide nanoparticles were incorporated into organic PMMA matrix.

Obtained images of optical microscopy showed that the embedded nanoparticles in polymer matrix are homogenous, for zirconia oxide nanoparticles than titanium oxide nanoparticles.

Micro Vickers hardness of ZrO_2 and ZrO_2-PMMA samples was determined and showed improved hardness of the samples with zirconia oxide nanoparticles on micro-level.

References

[1]. Zarb G., Bolender C., Eckert S. E., *Prosthodontic Treatment for Edentulous Patients: Complete Dentures and Implant-Supported Prostheses*, 13th ed., US Mosby,135, eBook ISBN: 978032309628, 2013.

[2]. Katja K., Lippo V., Lassila K., *Flexural fatigue of denture base polymer with fiber-reinforced composite reinforcement*, Compos Part A Appl Sci Manuf., 36, p.1177-1324, 2005.

[3]. Gaharwar K., Peppas N. A., Khademhosseini A., *Biotechnology and Bioengineering*, 111, (3), 441, 2014.

[4]. Zhang X.-Y., Zhang X.-J., Huang Z.-L., Zhu B.-S., Chen R.-R., *Hybrid effects of zirconia nanoparticles with aluminum borate whiskers on mechanical properties of denture base resin PMMA*, Dent. Mater. J., 33, p. 141-146, 2014.

[5]. Wang T., Tsoi J. K.-H., Matinlinna J. P., *A novel zirconia fibre-reinforced resin composite for dental use*, J. Mech. Behav. Biomed. Mater., 53 (Suppl. C), p. 151-160, 2016.

[6]. Kawai N., Lin J., Youmaru H., Shinya A., Shinya A., *Effects of threeluting agents and cyclic impact loading on shear bond strengths to zirconia with tribochemical treatment*, J. Dent. Sci., 7, p. 118-124, 2012.

[7]. Damian W., Michalmazur I., Joanna I., Aleksandra J., Malgorzata K., Piotr D., Danuta K., Jarosław D., *Mechanical and structural properties of titanium dioxide deposited by innovative magnetron sputtering process*, Materials Science-Poland, 33(3), p. 660-668, 2015.

[8]. Gao F. M., Gao L. H., *Microscopic Model of Hardness*, J. Superhard Mater., 32(3), 148, 2010.

[9]. Kulikovsky V., Ctvrtlik R., Vorlicek V., Filip J., Bohac P., Jastrabik L., *Mechanical properties and structure of TiO_2 films deposited on quartz and silicon substrates*, Thin Solid Films, 542, 91, 2013.

[10]. Zhang Q., Zhao Y., Jia Z., Qin Z., Chu L., Yang J., Zhang J., Huang W., Li X., *High stable, transparent and conductive ZnO/Ag/ZnO nanofilm electrodes on rigid/flexible substrates*, Energies, Doi: 10.3390/en9060443, 2016.

[11]. Gad M. M., Fouda S. M., Al-Harbi F.A., Näpänkangas R., Raustia A., *PMMA denture base material enhancement: a review of fiber, filler, and nanofiller addition*, Int J Nanomed., 12, p. 3801-3812, 2017.

[12]. Ayad N. M., Badawi M. F., Fatah A. A., *Effect of reinforcement of high impact acrylic resin with micro-zirconia on some physical and mechanical properties*, Rev Clin Pesq Odontol., 4(3), p. 145-151, 2008.

THE ANNALS OF "DUNAREA DE JOS" UNIVERSITY OF GALATI
FASCICLE IX. METALLURGY AND MATERIALS SCIENCE
N°. 3 - 2019, ISSN 2668-4748; e-ISSN 2668-4756
Article DOI: https://doi.org/10.35219/mms.2019.3.03

STUDY ON THE SLUDGE CAPITALIZATION AS A FERTILIZER FOR ORNAMENTAL GARDEN PLANTS

Adrian LEOPA, Anca SERBAN, Mariana Carmen BURTEA, Petru GOJAN
"Dunarea de Jos" University of Galati, Romania
e-mail: adrian.leopa@ugal.ro, anca.serban@ugal.ro, carmen.burtea@ugal.ro

ABSTRACT

The paper aimed to demonstrate that the sludge from wastewater treatment plants can be used efficiently as a fertilizer in horticulture because in the near future the storage of this sludge will become a problem. For this reason, we approached the study on the recovery of the sludge from the wastewater treatment plant of Brăila as fertilizer in the crops of ornamental garden plants that are not intended for consumption. The correct management of the sludge from wastewater treatment plants may bring a positive contribution to the vegetation development rate. The main objective of the sludge treatment is the capitalization and the decrease of negative impact on the environment.

KEYWORDS: wastewater, sludge, ornamental plants, fertilizer

1. Introduction

There are a number of scientific researches whose main objective is to identify economical and non-polluting solutions for the recovery of the sludge resulting from the wastewater treatment process. Thus, at the national level these concerns have materialized in the form of scientific papers, doctoral theses, monographs.

A PhD thesis [1] has investigated experimentally the possibility of dewatering the sludge from wastewater treatment by three methods of reducing its volume, as follows:

- alternative freeze-thaw cycles;
- chemical conditioning according to the KemiCond recipe followed by mechanical dehydration;
- microwave irradiation.

Another PhD thesis [2] studied the problem of the influence of sludge from urban wastewater treatment plants on lucerne (Medicago sativa) culture.

The increase of the urban population of Romania, but also requirements of the European Community regarding the recovery of the urban waste, have led to finding solutions for the implementation in the agricultural production systems of the urban sludge.

This sludge contains nutrients necessary for plant growth, and their use retains the phosphates' mineral reserves on which the phosphorus fertilizers are prepared. The physical, chemical and biological soil properties are improved by using this sludge. Although the fertilizing value of the sludge is generally recognized, the generalization of its use in agriculture has some objections regarding hygienic and sanitary aspects as well as the presence of unwanted elements such as: heavy metal compounds, pesticides and some non-degradable organic substances.

At the base of all sludge treatment processes are two distinct technological processes: the stabilization of the sludge by fermentation and the sludge dehydration. Most wastewater treatment plants in Romania are provided with mechanical and biological stages. The mechanical stage includes: the rare and thick grills, slime separator, pumping stations, primary decanters. Biological stage is composed of: aeration tanks, secondary decanters, pumping station, recirculated sludge and excess sludge. In most cases dewatering sludge from sewage treatment plants is carried out on drying beds. The new projects provided for the sludge dewatering by mechanical methods of centrifugation and press filters.

Regarding the heavy metals, the Directive 86/278/CEE stipulate for the concentration values in soils receiving sewage sludge, also their concentration in sewage sludge intended for agriculture capitalization and the annual maximum quantities of heavy metals that can reach agricultural soils.

The sludge from wastewater treatment with a composition similar to urban wastewater can be used in agriculture only if they comply with the present

THE ANNALS OF "DUNAREA DE JOS" UNIVERSITY OF GALATI
FASCICLE IX. METALLURGY AND MATERIALS SCIENCE
Nº. 3 - 2019, ISSN 2668-4748; e-ISSN 2668-4756
Article DOI: https://doi.org/10.35219/mms.2019.3.03

technical norms. On the agricultural lands can be applied only sludge with a certain content in polluting elements that do not exceed the limits of Table 1 [3].

Table 1. *The Maximum admissible values of heavy metals from sludge intended for use in agriculture (mg/kg dry matter)*

Parameters	Values
Cadmium	10
Copper	500
Nickel	100
Plumb	300
Zinc	2,000
Mercury	5
Chromium	500
Cobalt	50
Arsenic	10
AOX (sum of organohalogenated compounds)	500
PAHs (polycyclic aromatic hydrocarbons)	5
Polychlorinated biphenyls (PCBs)	0.8

The sewage sludge producers shall regularly provide for the sludge users the sludge supplies and characteristics as follows: pH, humidity, loss of ignition at 550 ºC (volatile substances in suspension), total organic carbon, nitrogen, phosphorus, potassium, cadmium, chromium, copper, mercury, nickel, plumb, zinc.

The sewage sludge application is allowed only in the period characterized by a regular access on the land and the soil sludge incorporation promptly after application.

The following rules are applied in the use of sludge:

- the nutritional requirements of the plants;
- the quality of soils and water surface will not be affected;
- the pH value of soils on which the sewage sludge will be applied should be kept above 6.5.

2. Materials and methods

The sewage sludge from the wastewater treatment plant of Braila was used in order to find its influence on the growth rate of ornamental garden plants. The sludge was already dehydrated when it was brought to be mixed with soil in different proportions.

The humidity and sun exposure conditions were the same. In each flowerpot were planted two seedlings.

The seedlings of ornamental plants Gazania talent yellow were planted on May 6, 2017 in number of 12, at the same vegetation stage as follows:

a. Variant V1 - 3 flowerpots 85% filled up with fertile soil and 15% sewage sludge, Fig. 1.

b. Variant V2 - 3 flowerpots 90% filled up with fertile soil and 10% sewage sludge, Fig. 2.

c. Variant V3 - 3 flowerpots 95% filled up with fertile soil and 5% sewage sludge, Fig. 3.

d. Variant V4 - 3 flowerpots filled up with fertile soil, Fig. 4.

Fig. 1. *Variant V1-the initial seeding phase*

Fig. 2. *Variant V2 - the initial seeding phase*

Fig. 3. *Variant V3 - the initial seeding phase*

Fig. 4. *Variant V4 - the initial seeding phase*

THE ANNALS OF "DUNAREA DE JOS" UNIVERSITY OF GALATI
FASCICLE IX. METALLURGY AND MATERIALS SCIENCE
N°. 3 - 2019, ISSN 2668-4748; e-ISSN 2668-4756
Article DOI: https://doi.org/10.35219/mms.2019.3.03

Fig. 5. *Variant 1, 2, 3, 4 –overall view of the initial seeding phase*

One of the chosen parameters for the comparative assessment of the plants growth rate of the four variants is the plant's epigean part. Thus, after planting the twelve seedlings of Gazania talent yellow, the plant's epigean parts were measured as seen in Table 2.

Table 2. *The length of the plant's epigean part at the planting date*

The length of the plant's epigean part												
Date of measurement: 06.05.2017												
Variant No.	V1			V2			V3			V4		
Seedling No.	1	2	3	4	5	6	7	8	9	10	11	12
Seedling 1 -left	70	75	55	65	100	70	85	75	70	65	90	75
Seedling 2 -right	60	60	65	65	100	80	95	95	60	75	85	80

Based on the average values (Table 3) the chart for the differences assessment regarding the growth rate of the plants have been achieved.

Table 3. *The length of the plant's epigean part one month after planting*

Date of measurement: 06.06.2017												
Variant No.	V1			V2			V3			V4		
Seedling No.	1	2	3	4	5	6	7	8	9	10	11	12
Seedling 1 -left	80	100	120	dry	160	140	160	90	150	170	140	120
Seedling 2 -right	100	135	135	dry	150	85	150	135	105	150	160	150

The most important percentage increase was the seedings from the control sample followed in descending order by variants 1, 3 and 2.

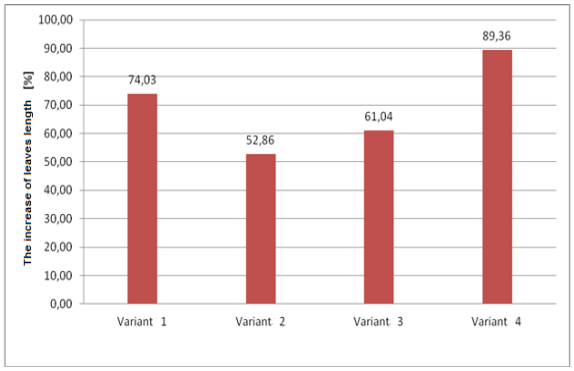

Fig. 6. *The percentage increase of the epigean part for the four variants*

3. The study results

At 50 days after planting, four representative flowerpots were selected from the four variants, namely flowerpot 2, 6, 8, 12, and a typical plant from each flowerpot was selected.

Fig. 7. *Variant V1 - end of growing season*

Fig. 8. *Variant V2 - end of growing season*

THE ANNALS OF "DUNAREA DE JOS" UNIVERSITY OF GALATI
FASCICLE IX. METALLURGY AND MATERIALS SCIENCE
N°. 3 - 2019, ISSN 2668-4748; e-ISSN 2668-4756
Article DOI: https://doi.org/10.35219/mms.2019.3.03

Fig. 9. *Variant V3 - end of growing season*

Fig. 10. *Variant V4 - end of growing season*

Fig. 11. *Variant 1, 2, 3, 4 - end of growing season*

For the four plants the following growth - related parameters of the plants of Gazania Talent Yellow were evaluated:

- the flower number;
- the flowers diameter;
- the length of the flower shank;
- the length of the epigean part of full-blown leaves;
- the length of the epigean part of decorative flowers.

In order to provide a better possibility of comparing the results from evaluation of the parameters, they will be presented in a table for the four cases considered.

The characteristic parameters for the Gazania flowers were the following:

- the number of blooming flowers;
- the number of flower buds;
- the flowers diameter;
- the length of the flower shank;
- the shank flowers mass.

Table 4. *The characteristic parameters of the Gazania flowers*

Variant No. / % sludge	Number of blooming flowers [piece]	Number of flower buds [piece]	Flowers diameter [cm]	Length of the flower shank [cm]	Shank flowers mass [g]
2 / 15% sludge	3	3	5,3	13,5	14,6
6 / 10% sludge	3	0	5	12	17,3
8 / 5% sludge	4	2	5,3	12,5	16,2
12 / control sample	3	0	5	14,4	8

flowerpot 2

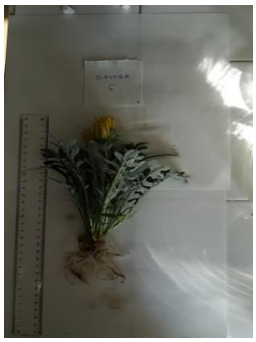

flowerpot 6

flowerpot 8

flowerpot 12

Fig. 12. *The typical plants of the representative flowerpots*

THE ANNALS OF "DUNAREA DE JOS" UNIVERSITY OF GALATI
FASCICLE IX. METALLURGY AND MATERIALS SCIENCE
Nº. 3 - 2019, ISSN 2668-4748; e-ISSN 2668-4756
Article DOI: https://doi.org/10.35219/mms.2019.3.03

Considering the results set out above, it can be stated that the variant using just 5% sludge (Table 4) had brought the best results regarding the characteristic parameters of the Gazania flowers.

The variant with the most decorative leaves is the one that has in the substrate composition a percentage of 5% sludge (Table 5). It should be mentioned that the variant with the most mature and decorative leaves is the one with 15% sludge in the composition.

The analysis of the obtained values reveals that from a mass point of view the mixture with a percentage of 5% sludge (Table 6) favored the development of the plants planted in it.

Table 5. *The characteristic parameters of the Gazania leaves*

Flowerpot No. / % sludge	Number of mature leaves [piece]	Number of decorative flower [piece]	Mature leaves mass [g]	Decorative leaves mass [g]
2 / 15% sludge	13	27	5,6	14,8
6 / 10% sludge	5	26	3,7	24,8
8 / 5% sludge	4	26	1,7	34
12 / control sample	6	3	2,9	1,1

Table 6. *The plants weight parameters*

Flowerpot No. / % sludge	The root mass [g]	The whole plant mass [g]
2 / 15% sludge	5,6	39,2
6 / 10% sludge	2,9	50,2
8 / 5% sludge	4,4	56,5
12 / control sample	1,4	13,4

4. Conclusions

The proper management of the sludge from the wastewater treatment plants can bring a positive contribution to agriculture, which is also obvious from the work carried out. Using small percentages of sewage sludge mixed with the soil can bring encouraging results. When used in large percentages, sludge is not a viable solution for plant development.

Considering that in the near future the sludge from municipal wastewater treatment plants will no longer be able to be deposited in landfills, it is imperative to identify alternatives for its capitalization.

The use of sewage sludge as a fertilizer for garden decorative plants can be a solution for capitalization only for part of its volume. As for garden decorative plants, the pathogenic potential of the sludge used as fertilizer is eliminated.

The experimental part carried out in this work pointed out that the mixture obtained from 5% sewage sludge and 95% fertile soil ensures the most favorable development for the Gazania Talent Yellow ornamental plant. This finding recommends the use of sewage sludge as a fertilizer for ornamental plants planted in specially designed spaces in the municipality of Braila. As a safety measure, in order to prevent the direct contact with the sludge it is proposed that the mixture of the sludge and soil it is covered with a layer of fertile soil with a thickness of 50-60 mm.

References

[1]. Iorgulescu M., *Tratarea nămolurilor provenite de la statiile de potabilizare a apei*, Teză de doctorat, Facultatea de Hidrotehnică, Universitatea Tehnică de Construcţii din Bucureşti, 2015.

[2]. Pintea I. I., *Cercetări privind influenţa nămolurilor de la staţiile de epurare orăşeneşti asupra culturii de lucernă*, Teză de doctorat, Universitatea de ştiinţe agricole şi medicină veterinară Cluj-Napoca, 2012.

[3]. ***, *NORME TEHNICE din 16 august 2004 privind protecţia mediului şi în special a solurilor, când se utilizează nămolurile de epurare în agricultură*.

THE ANNALS OF "DUNAREA DE JOS" UNIVERSITY OF GALATI
FASCICLE IX. METALLURGY AND MATERIALS SCIENCE
N°. 3 - 2019, ISSN 2668-4748; e-ISSN 2668-4756
Article DOI: https://doi.org/10.35219/mms.2019.3.04

REVIEW ON THE ELABORATION AND MORFO-STRUCTURAL CHARACTERIZATION OF IRON OXIDE FOR CATALYTIC APPLICATIONS

Ecaterina Magdalena MODAN, Adriana-Gabriela PLĂIASU
University of Pitesti, Pitesti, Romania
e-mail: ecaterina.modan@upit.ro, gabriela.plaiasu@upit.ro

ABSTRACT

Magnetite, Fe_3O_4 exhibits the strongest magnetism of transition metal oxides. Hematite, α-Fe_2O_3 being the most stable oxide and semiconductor type n under environmental conditions, can be widely used in catalysts, pigments and gas sensors. Iron oxide nanoparticles (Fe_3O_4 and γ-Fe_2O_3) with superparamagnetic properties and low toxicity, are particularly useful for catalytic applications especially in the medical field. For these applications, the Fe_3O_4 and γ-Fe_2O_3 nanoparticles are usually smaller than 20 nm, where they have superparamagnetic properties, i.e. a high magnetic saturation moment and almost zero coercivity. This review presents the theoretical concepts of the structure properties of this oxide and the elaboration methods that make iron oxide the ideal candidate for catalytic applications.

KEYWORDS: iron oxide, hematite, magnetite, maghemite, properties, morphologies, elaboration

1. Introduction

Iron oxide is a naturally occurring mineral compound that has several crystalline structures and also different structural and magnetic properties [1]. The main crystalline forms of this mineral are: hematite (α-Fe_2O_3); magnetite (Fe_3O_4); maghemite (γ-Fe_2O_3) [2].

Hematite (α-Fe_2O_3) is the mineral form of iron oxide III. It is found in soils and has different colours from black to silver-grey, maroon to reddish or even red. Hematite (α-Fe_2O_3) can be widely used in catalysts, pigments and gas sensors, as it is the most stable iron oxide and n-type semiconductor [3]. Hematite is easier to synthesize than other forms of oxide, as it is the end product of other forms of iron oxide transformation and is also extremely stable under environmental conditions. It can also be used as a basic material for the synthesis of magnetite (Fe_3O_4) and maghemite (γ-Fe_2O_3) [4]. As shown in Figure 1 (a), α-Fe_2O_3 has a rhombohedral structure. Magnetite (Fe_3O_4) is a magnetic iron oxide nanoparticle known as black iron oxide, magnetic iron ore. Among the transition metal oxides, it exhibits the strongest magnetism [5]. Fe_3O_4 has the spinel structure, exemplified in Figure 1. Fe_3O_4 differs from most other iron oxides in that it contains both divalent and trivalent iron. Thus, Fe_3O_4 can be both a n-type and p-magnetic semiconductor (Fe_3O_4), at room temperature, having ferromagnetic properties, which differs from other forms of iron oxides, because its structure has both divalent and trivalent iron. However, Fe_3O_4 has the lowest resistivity among iron oxides due to low bandgap (0.1 eV) [6].

Maghemite (γ-Fe_2O_3) is one of the magnetic forms of iron oxides and has a brown colour. The structure of the maghemite is a cubic spinel structure, and for this reason it can be regarded as a magnetite with Fe^{2+} deficiency. Therefore, maghemite can be considered as completely oxidized magnetite and is a n-type semiconductor with a 2.0 eV band [7].

The crystalline structures of iron oxide are exemplified in Fig. 1 [8].

Due to their superparamagnetic properties and low toxicity, iron oxide nanoparticles (Fe_3O_4 and γ-Fe_2O_3) are particularly interesting for biomedical applications, such as NMR imaging. For these applications, the Fe_3O_4 and γ-Fe_2O_3 nanoparticles are usually smaller than 20 nm, have superparamagnetic properties, i.e. high magnetic saturation moment and almost zero coercivity.

THE ANNALS OF "DUNAREA DE JOS" UNIVERSITY OF GALATI
FASCICLE IX. METALLURGY AND MATERIALS SCIENCE
N°. 3 - 2019, ISSN 2668-4748; e-ISSN 2668-4756
Article DOI: https://doi.org/10.35219/mms.2019.3.04

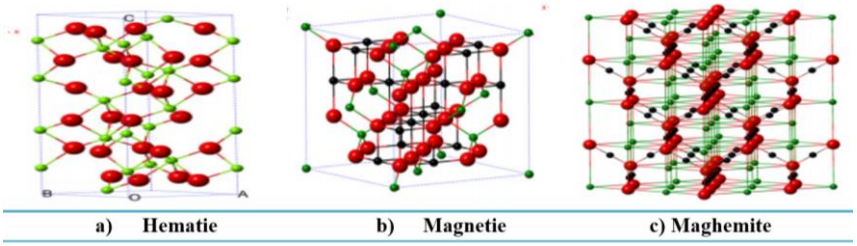

Fig. 1. *Crystal structures of hematite, magnetite and maghemite (● -Fe^{2+}, ● -Fe^{3+}, ● - O^{2-})* [8]

Magnetite is a very promising iron oxide due to its proven biocompatibility. Magnetic nanoparticles of iron oxides have excellent applications in drug delivery to tumours as well as anticancer agents [9-14]. Magnetite and hematite have been used as catalysts for a number of industrially important reactions, including desulfurization of natural gas synthesis, high temperature water change reaction and in the Haber process. They are also involved in the oxidation of alcohols and the large-scale manufacture of butadiene [10-16]. Maghemite has applications in data recording and storage [17]. All three forms of magnetic iron oxide are commonly used in synthetic pigments, paints, ceramics and porcelain [18]. In recent decades, special attention has been focused on the development of elaboration approaches to produce nanoparticles that are shape and size controlled, biocompatible and monodisperse for catalytic applications [19]. Various morphologies of iron oxide nanoparticles (nanospheres, plates, tetrahedrons, cubes, nanowires, nanotubes, nanoflowers, nanoins) have been developed according to different synthesis protocols and are exemplified in Figure 2 [20-21].

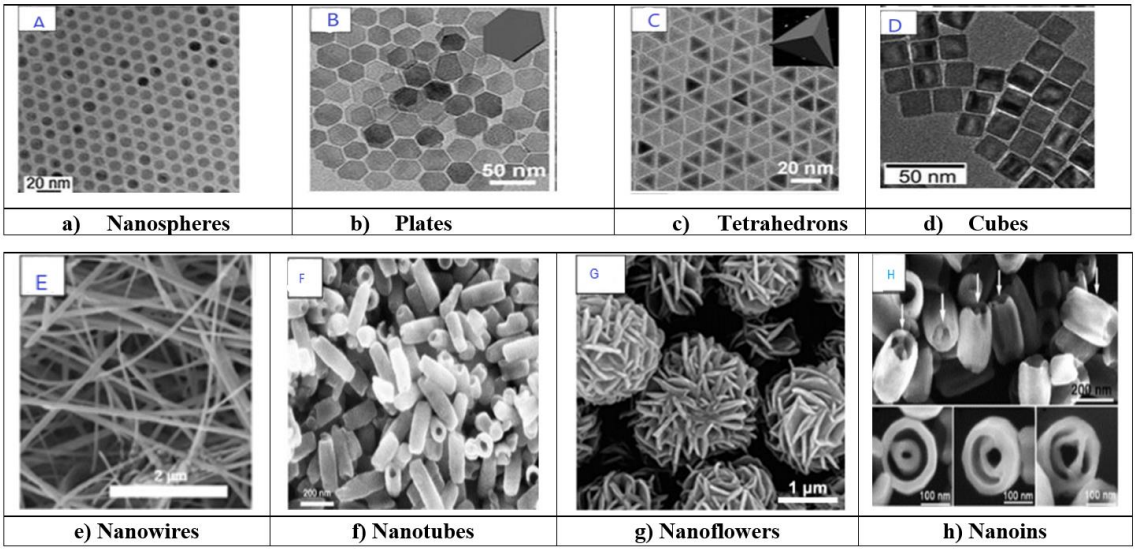

Fig. 2. *Morphologies of iron oxide nanoparticles (a) nanospheres, (b) plates, (c) tetrahedrons, (d) cubes (e) nanowires, (f) nanotubes, (g) nanoflowers, (h) nanoins* [20, 21]

2. Methods of elaboration

2.1. Precipitation method

The most commonly used method for obtaining Fe_xO_y is co-precipitation. The method consists of mixing precursors containing Fe^{2+}/Fe^{3+} = 1:2 in basic solutions at room temperature or at high temperature. The size and morphology of iron oxide nanoparticles depend on the type of salt used, chlorides, sulphates, nitrates, perchlorates, etc., the ratio of Fe^{2+}/Fe^{3+} concentration, the reaction temperature, the pH value, the ionic resistance of the environment and the other reaction parameters (e.g. stirring speed, lowering rate of the basic solution). In 1981, the development of superparamagnetic iron oxide nanoparticles with controlled dimensions was reported by precipitation in basic environment of $FeCl_3$ and $FeCl_2$ salts by Massart and his collaborators. They observed the influence of the base used (ammonia, methylamine and sodium hydroxide), the pH value, the Fe^{2+}/Fe^{3+} ratio on the reaction yield, the diameter and the

THE ANNALS OF "DUNAREA DE JOS" UNIVERSITY OF GALATI
FASCICLE IX. METALLURGY AND MATERIALS SCIENCE
N°. 3 - 2019, ISSN 2668-4748; e-ISSN 2668-4756
Article DOI: https://doi.org/10.35219/mms.2019.3.04

polydispersity of the obtained nanoparticles. By adjusting these parameters, nanoparticles with sizes from 4.2 nm to 16.6 nm were obtained. XRD data revealed a rhombohedral (hexagonal) structure with space group R-3c in all samples. TEM and SEM confirmed the spherical morphology of precipitated synthesized iron oxide nanoparticles [23, 24]. Sun and Zeng developed magnetic nanoparticles of magnetite with variable dimensions from 3 nm to 20 nm in diameter by co-precipitating a stoichiometric mixture of Fe (II) and Fe (III) salts in a basic medium, sodium hydroxide or ammonium hydroxide. Both high-resolution TEM HRTEM and XRD were used to obtain information about nanoparticle structure (Fe_3O_4). The spherical morphology with the size around 20 nm of iron oxide nanoparticles was determined by SEM [25].

Table 2. *Reaction parameters and characterization of iron oxide nanoparticles obtained by co-precipitation method*

Oxide type	Precursor	Hydrolysis agent / surfactant / solvent	Temperature Time pH	Dimension/ morphology	Characterization method	References
Fe_3O_4	$FeCl_3 \cdot 6H_2O$ $FeCl_2 \cdot 4H_2O$	NH_3 NaOH CH_3NH_2	25	4.2-16.6 nm/ spheres	XRD, SEM	[23, 24]
Fe_3O_4	$FeCl_3 \cdot 6H_2O$ $FeCl_2 \cdot 4H_2O$	NaOH NH_4OH	25 °C	3-20 nm spheres	XRD, TEM	[25]
Fe_3O_4	$FeCl_2$ $FeCl_3$	Na OH	25 °C pH = 11-12	8.5 nm/ spheres	XRD, TEM	[26]
Fe_3O_4	$FeCl_3 \cdot 6H_2O$ $FeCl_2 \cdot 4H_2O$	NH_3	25 °C 60 min pH = 1.5-9	40 nm/ spheres	SEM, TEM, XRD	[27-28]
α-Fe_2O_3	$FeCl_3 \cdot 6H_2O$	NaOH NH_4OH	80 °C pH = 11	21-82 nm	SEM, TEM, XRD	[29]
Fe_3O_4	$FeCl_3 \cdot 6H_2O$	KI NH_3 PVA	Calcination 250 °C	7.84 nm / spheres d = 6.3 nm, l = 46.2/ nanorods	SEM, TEM, XRD	[30]

Kang *et al.* have synthesized monodisperse, uniform, narrow-size nanoparticles of Fe_3O_4 by co-precipitation without surfactants, using iron chlorides with a molar ratio of Fe^{II} / Fe^{III} = 0.5 to a pH = 11-12. XRD data revealed a cubic structure. The spherical morphology with the size around 8.5 nm of the iron oxide nanoparticles was determined SEM [26]. Ahn *et al.* have obtained magnetite by this method and demonstrated that different iron species (oxyhydroxide) compositions can result. Mainly, the composition and also the size of the magnetite strongly depend on the molar ratio Fe^{2+}/ Fe^{3+}. The small values of the ratio x = Fe^{2+}/ Fe^{3+} which is x less than 0.1 lead to the formation of goethite [FeO(OH)]. For x = 0.2 and x = 0.3, the distinct phase of oxyhydroxide and the variable size of the non-stoichiometric magnetite were formed. However, the best-known molar ratio used is x = 0.5 producing homogeneous nanoparticles in size and composition. The morpho-structural characterization of the synthesized iron oxide hydroxide nanoparticles was performed by XRD, TEM, SEM. XRD data revealed an orthorhombic structure. The 40 nm spherical morphology of iron oxide nanoparticles was determined by SEM [27, 28].

Lassoued *et al.* have reported the elaboration of α-Fe_2O_3 hematite nanoparticles by a simple chemical method of co-precipitation starting from the hexahydrated iron chloride precursor. They followed in the experiments the impact of the variation of the precursor concentration on the crystalline phase, the size and the morphology of α-Fe_2O_3. The characteristics of the synthesized hematite nanoparticles were evaluated by XRD, TEM, SEM. XRD data revealed a rhombohedral (hexagonal) structure with space group R-3c in all samples. TEM

THE ANNALS OF "DUNAREA DE JOS" UNIVERSITY OF GALATI
FASCICLE IX. METALLURGY AND MATERIALS SCIENCE
N°. 3 - 2019, ISSN 2668-4748; e-ISSN 2668-4756
Article DOI: https://doi.org/10.35219/mms.2019.3.04

and SEM were confirmed by the uniform spherical morphology. The result revealed that the particle sizes varied between 21 nm and 82 nm and the increase of the precursor concentration ($FeCl_3 \cdot 6H_2O$) was accompanied by an increase of the particle size of 21 nm for pure α-Fe_2O_3 synthesized with [Fe^{3+}] = 0.05 M at 82 nm for pure α-Fe_2O_3 synthesized with [Fe^{3+}] = 0.4 M [29].

Instead of using two iron precursors, Khalil started from an aqueous solution of Fe^{3+} salt. The procedure consisted of mixing iron chloride with an aqueous solution of potassium iodide with a 3:1 molar ratio. Potassium iodide reduces iron salt. The mixture was hydrolyzed with 25% ammonia to obtain the black precipitate of magnetite. He obtained spherical magnetite nanocrystals with a diameter of 7.84 nm, rods with a diameter of 6.3 nm and a length of 46.2 nm. The morphology of Fe_3O_4 nanocrystals was examined with the scanning electron microscope and a transmission electron microscope with an acceleration voltage of 200 kV [30].

Kirillov *et al.* have obtained magnetite nanoparticles by co-precipitating iron sulphate (II) and iron chloride (III) in the presence of citrate ions, at room temperature and in argon medium. By changing the molar concentration of citrate, it was possible to obtain nanoparticles of different sizes (from 10.5 nm to 4.4 nm) demonstrated by scanning electron microscopy [31]. Table 2 shows the precursors, hydrolysis agents, surfactants, solvents, reaction conditions, dimensions and morphologies of iron oxides elaborated by coprecipitation method.

2.2. Thermal decomposition

Thermal decomposition is one of the most studied methods for the controlled elaboration of different types of nanoparticles. The elaboration of nanoparticles by thermal decomposition is based on the thermal decomposition of the various iron precursors (salts or complex combinations) in organic environment and at high temperature. As an organic medium, high boiling solvents and surfactants are used. The morphology and size of the elaborated nanoparticles can be influenced by the ratio between the reactants used in the reaction, the temperature and the reaction time [31].

Rockenberge *et al.* have developed γ-Fe_2O_3 with a size of 10 nm by thermal decomposition starting from the precursor of the iron-cupferon complex (Cup = N-nitroso-phenylhydroxylamine-$C_6H_5N(NO)OH$) [32].

Shortly, the Hyeon-led group of researchers developed iron oxide nanoparticles using the thermal decomposition method based on heating a reaction mixture (precursor, solvent, and surfactants) to the reflux temperature of the solvent (typically chain hydrocarbons are used) such as 1-octadecen, 1-eicosan, etc.). Monodisperse magnetite with a particle size of 12 nm was prepared starting from the iron-oleate complex, oleic acid which was dissolved in 200 g of 1-octadecene at room temperature. The mixture was heated at 320 °C for 30 min. When the reaction temperature reached 320 °C, the initial solution that was transparent became black-brown. The resulting solution containing the nanocrystals was then cooled to room temperature. Iron oxide nanocrystals were separated by centrifugation and characterized by XRD and TEM [33].

Maity *et al.* have studied the influence of reaction time on the size of nanoparticles developed by the thermal decomposition method. To obtain magnetite, the authors started from a mixture of iron acetylacetonate, oleic acid and oleylamine. If the reaction was carried out at 300 °C for 30 min, 5 nm nanoparticles were synthesized. By increasing the reaction time to 2 h, the size of the nanoparticles increased to 6 nm and after 24 h to 11 nm. If the elaboration reaction of the magnetite nanoparticles took place at 330 °C, varying the reaction time from 30 min to 7 h, spherical nanoparticles from 7 nm to 11 nm were obtained, demonstrated by electron microscopy characterization of sweeps [34, 35].

Colvin et al have demonstrated the possibility of combining both precursor and particle synthesis in a single process, using FeO(OH) as an iron source. In this process, a mixture of FeO(OH), oleic acid and 1-octadecene is heated for several hours, which results in the synthesis of nanoparticles with monodisperse magnetite. The particle size increases linearly as the molar ratio of oleic acid / FeO(OH) becomes larger. Also, by raising the temperature to 340 °C, particles with dimensions larger than 20-30 nm were developed, but at higher temperature the particle size distribution is considerably affected. TEM microscopy of these nanocrystals demonstrates the high quality of the synthesized nanocrystals. XRD confirms the magnetite crystal structure of the obtained nanocrystals.

Another research for the development of magnetic nanoparticles of 4nm size was proposed by Sun *et al.* who have heated a mixture of iron acetylacetonate, phenyl ether, 1,2-hexadecanediol, oleic acid and oleylamine at reflux for half an hour. The uniform magnetic nanoparticles were synthesized by the decomposition of the organometallic precursors in an organic medium and in the presence of a surfactant, such as oleic acid. Higher temperatures, higher iron concentrations have been shown to accelerate the reaction and induce smaller particles and the oleic acid coating appears to be responsible for very high saturation magnetization values, independent of particle size and decreasing

THE ANNALS OF "DUNAREA DE JOS" UNIVERSITY OF GALATI
FASCICLE IX. METALLURGY AND MATERIALS SCIENCE
N°. 3 - 2019, ISSN 2668-4748; e-ISSN 2668-4756
Article DOI: https://doi.org/10.35219/mms.2019.3.04

coercivity values, with the reduction of the particle size [36].

Table 3 illustrates precursors, hydrolysis agents, reaction parameters, characterization methods, crystallite dimensions of iron oxides obtained by the thermal decomposition method.

Table 3. *Precursors, hydrolysis agents, reaction parameters and characterization of iron oxide nanoparticles obtained by the thermal decomposition method*

Oxide type	Precursor	Hydrolysis agent / surfactant / solvent	Temperature	Dimension/ morphology	Characterization method	References
Fe_3O_4	Iron cupferon	octylamine	250-300 °C	10 nm	XRD, SEM	[32]
Fe_3O_4	Iron Oleat Complex	1-octadecene Oleic acid	320 °C	12 nm	XRD, TEM	[33]
Fe_3O_4	Iron acetylacetonate	oleylamine Oleic acid	300-330 °C	7-11 nm	XRD, TEM	[34]
Fe_3O_4	Iron hydroxide oxide	Oleic acid 1-octadecene	340 °C	20-30 nm	XRD, TEM	[35]
γ-Fe_2O_3	Iron acetylacetonate	phenyl ether of oleic acid oleylamine	265 °C	4 nm	XRD, TEM	[36]

2.3. Sol-gel method

Cui *et al.* were able to develop different iron oxide nanoparticles α-Fe_2O_3, γ-Fe_2O_3 and Fe_3O_4 almost monodisperse through a medium-temperature sol-gel route. The formation of the various final iron oxide structures depends only on the drying process. Through TEM analysis, Cui *et al.* have observed 4.9 nm Fe_3O_4 nanoparticles that were obtained by soil centrifugation. When the xerogel was heated to 150 °C, a slight increase in γ-Fe_2O_3 size formed. However, direct drying at 150 °C of the wet Fe_3O_4 gel allowed for the first time to transform into α-Fe_2O_3 with a size of 10.1 nm. The XRD models of the samples were measured with a diffractometer, the size of the crystallite was calculated using the Scherrer equation. The observation of the particle morphology was performed on a transmission electron microscope. The powder sample was carefully ground, then dispersed in ethanol by ultrasound. In the case of Fe_3O_4, the particles contained on the copper grid were introduced into the TEM test chamber immediately after the vacuum dried sample, avoiding the oxidation of Fe_3O_4. Particle size distributions were obtained by counting approximately 500 nanoparticles from TEM images [37]. The combination of microwave assisted heating with the sol gel method offers a quick and efficient synthesis methodology. For example, the researcher Bilecka together with his collaborators developed iron oxide nanoparticles, Fe_3O_4 with dimensions of 5-11 nm using as an iron acetylacetonate precursor which dissolved in benzyl alcohol and was heated to 170 °C by radiation exposure with microwave for 12 min [38].

Table 4 illustrates precursors, hydrolysis agents, reaction parameters, characterization methods, dimensions and morphologies of iron oxides obtained by the sol-gel method.

Table 4. *Precursors, hydrolysis agents, reaction parameters and characterization of iron oxide nanoparticles obtained by sol-gel method*

Oxide type	Precursor	Hydrolysis agent / surfactant / solvent	Temperature Time	Dimension/ morphology	Characterization method	References
Fe_3O_4	Iron acetylacetonate	Benzyl alcohol	12 min	11 nm 7 nm 5 nm/spheres	SEM, TEM, XRD	[37]
Fe_3O_4 **α-Fe_2O_3** **γ-Fe_2O_3**	$FeCl_2 \cdot 4H_2O$	ethanol	150 °C	4.9 nm 10.1 nm/spheres	SEM, XRD	[38]

THE ANNALS OF "DUNAREA DE JOS" UNIVERSITY OF GALATI
FASCICLE IX. METALLURGY AND MATERIALS SCIENCE
N°. 3 - 2019, ISSN 2668-4748; e-ISSN 2668-4756
Article DOI: https://doi.org/10.35219/mms.2019.3.04

2.4. Ultrasonic assisted hydrolytic synthesis

This method has been applied for the synthesis of various iron oxide nanoparticles. For example, magnetite can be produced by sonication of iron (II) acetate in water in an argon atmosphere.

Vijayakumar *et al.* have reported the synthesis of pure nanometric particles of Fe_3O_4 using iron (II) acetate as a precursor. Fe_3O_4 nano powders made of 10 nm size are superparamagnetic, and its magnetization at room temperature is very low around 1.25 g emu 1. The nanoparticles were characterized by elemental analysis, EDX, transmission electron microscopy, dynamic light scattering, Raman spectroscopy, XPS [39].

Amir *et al.* have developed the α-Fe_2O_3 nanocrystalline iron oxide using ultrasound irradiation for 1 hour using a suspension containing hexahydrated iron chloride and aqueous sodium hydroxide. Iron oxide nanoparticles were characterized by TEM, XRD. From TEM observations, the size of iron oxide nanoparticles is estimated to be significantly less than 19 nm. The powder X-ray diffraction data after annealing provide direct evidence that iron oxide formed during the sono-chemical process. They pointed out that high-energy ultrasound use produces spherical particles. The crystallite size varies between 5 nm and 7.5 nm for the different temperatures used. Research shows that the particle size is strongly dependent on the reaction temperature and the ultrasound intensity [40].

The α-Fe_2O_3 nanoparticles (hematite) were synthesized by the sono-chemical method by Azadeh *at el.* who have started from the precursors of iron acetate or iron chloride and sodium hydroxide with molar ratios of 1:2 or, respectively, 1:3, in 100 mL ethanol and water at a ratio of 1:3. The reactions were performed with ultrasound (with a frequency of 20 kHz and a power of approximately 150 W) at room temperature for 1 h. In all reactions, the intermediate was FeO(OH) nanoparticles. The precipitates were then calcined at 900 °C in an air atmosphere for 4 hours. XRD, SEM and IR spectroscopy were used to characterize the nanostructures. XRD data revealed a rhombohedral (hexagonal) structure with space group R-3c in all samples. TEM and SEM were confirmed by the uniform spherical morphology. The result revealed that the particle sizes varied between 13.02 nm and 79.197 nm [41]. Table 5 illustrates precursors, hydrolysis agents, reaction parameters, characterization methods, dimensions of iron oxides obtained by ultrasound.

Table 5. *Precursors, hydrolysis agents, reaction parameters and characterization of iron oxide nanoparticles obtained by US method*

Oxide type	Precursor	Hydrolysis agent / surfactant / solvent	Temperature Time	Dimension/ morphology	Characterization method	References
Fe_3O_4	$(AcCOO)_3Fe$	H_2O	25 °C 3 h	10 nm	SEM, TEM, XRD, DLS	[39]
Fe_3O_4 α-Fe_2O_3 γ-Fe_2O_3	$FeCl_3 \cdot 6H_2O$	NaOH	1 h	19 nm/spheres	SEM, XRD	[40]
α-Fe_2O_3	$Fe(C_2H_3O_2)_2$ sau $FeCl_3 \cdot 6H_2O$	NaOH	150 W 20 KHz 25 °C ,1 h	13.02 nm - 79.197 nm/ spheres	SEM, XRD, IR	[41]

4. Conclusions

From the analysis of the specialized scientific works regarding the elaboration and characterization of the iron oxide with catalytic applications, important elements regarding: the type of the synthesis, the methods of morpho-structural characterization have resulted.

Based on the analysis regarding the researches carried out on the synthesis and characterization of iron oxide, the following conclusions were drawn. Magnetite, Fe_3O_4, exhibits the strongest magnetism of transition metal oxides. Hematite, α-Fe_2O_3, being the most stable oxide and semiconductor type n under environmental conditions, can be widely used in catalysts, pigments and gas sensors. Iron oxide nanoparticles (Fe_3O_4 and γ-Fe_2O_3) with superparamagnetic properties and low toxicity, are particularly useful for catalytic applications especially in the medical field, such as magnetic resonance imaging (MRI). For these applications, the Fe_3O_4 and γ-Fe_2O_3 nanoparticles are usually smaller than 20 nm, where they have superparamagnetic properties, i.e. a high magnetic saturation moment and almost zero coercivity. Various morphologies of iron oxide

nanoparticles (nanospheres, plates, tetrahedra, cubes, nanowires, nanotubes, nanoflores, nanoins) have been elaborated according to different synthesis protocols. Methods for the production of titanium dioxide include chemical syntheses (hydrothermal, sol-gel, co-precipitation, sonochemistry, microwave assisted) using a variety of precursors of Fe^{2+}, Fe^{3+} salts (chlorides, sulphates, acetates, nitrates). The size of the iron oxide nanoparticles elaborated by the co-precipitation method varies from 3 nm to 82 nm. The size of the iron oxide nanoparticles synthesized by the thermal decomposition method varies from 4 nm to 30 nm. By the sol gel method, iron oxide nanoparticles were obtained, the size of which varies from 5 nm to 11 nm. The size of iron oxide nanoparticles elaborated by the sonochemistry method ranges from 10 nm to 79.197 nm. Iron oxide nanoparticles were characterized by transmission electron microscopy, X-ray diffraction, IR spectroscopy with Fourier transform.

References

[1]. Moura K. F., Maul J., Albuquerque A. R., Casali G. P., Longo E., Keyson D., Souza A. G., Sambrano J. R., I.M.G. J. Solid State Chem, 210, p. 171-177, 2014.
[2]. Babay S., Mhiri T., Toumi M., J Mol Struct, 1085, p. 286-293, 2015.
[3]. Machala L., Tucek J., Zboril R., Chem Mater, 23, (14), p. 3255-3272, 2011.
[4]. Zhang Z., Boxall C., Kelsall G. H., Colloids Surf., A 73, 145, 1993.
[5]. Wu W., Xiao X. H., Zhang S. F., Zhou J. A., Fan L. X., Ren F., Jiang C. Z., J. Phys. Chem. C, 114, 16092, 2010.
[6]. Teja S. A., Koh P. Y., Prog Cryst Growth Charact Mater, 55, p. 22-45, 2009.
[7]. Boxall C., Kelsall G., Zhang Z., J. Chem. Soc. Faraday Trans, 92, 79, 1996.
[8]. Wei Wu., Zhaohui Wu., Taekyung C. J., Woo S. K., Sci Technol Adv Mat, 16, 43, 2015.
[9]. Cullity B. D., AddisonWesley: Reading, MA., p. 9-80, 1972.
[10]. Salata O. V., J Nanobiotechnology, 2, 3, 2004.
[11]a. Jiang J. Z, Lin R., Lin W., Nielsen K., Mørup S., Dam Johansen K., Clasen R., J. Phys, 30, 1459, 1997.
[11]b. Sun H. T., Cantalini C., Faccico M., Peline M., J. Am. Ceram. Soc., 79, 927, 1996.
[11]c. Matijevic E., Scheiner P. J., Colloid Interface Sci., 63, 509, 1978.
[11]d. Ozaki M., Kratohvil S., Matijevic B., J. Colloid Interface Sci., 102, 146, 1984.
[12]a. Benz M., van der Kraan A. M., Prins. R, J. Appl. Catal. A., 172, 149, 1998.
[12]b. Anantharaman M. R., Joseph K. V., Keer H. V., Bull, Mater. Sci., 20, 975, 1997.
[12]c. Kryder M. H., MRS Bull 21, 17, 1996.
[12]d. Onodera S., Kondo H., Kawana T., MRS Bull, 21, 35, 1996.
[12]e. Watanabe H., Seto J., Bull. Chem. Soc. Jpn 61, 2411, 1991.
[12]f. Hong F. B., Yang L., Schwartz L. H., Kung H. H., J. Phys. Chem., 88, 2525, 1984.
[13]a. Lubbe A. S., Bergemann C., Brock F., McClure D. G., J. Magn. Magn. Mater, 194, 149, 1999.
[13]b. Popplewell J., Sakhnini L., J. Magn. Magn. Mater, 149,72, 1995.
[13]c. Pouliquen D., Perroud H., Calza F., Jallet P., Lejeune. J. Magn. Reson. Med., 24, 75, 1992.
[13]d. Lisiecki I., Billoudet F., Pileni M. P., J. Phys. Chem, 100, 4160, 1996.
[14]. Hibst H., Schwab E., Cahn R. W., VCH, Weinheim, 3B, 352, 1993.
[15]. Azhar Uddin M., Tsuda H., Wu S., E. Sasaoka 87, 451-459, 2008.
[16]. Li C., Shen Y., Jia M., Sheng S., Adebajo M. O., Zhu H., 9, 355-361, 2008.
[17]. Shi F., Tse M. K., Pohl M. M., Bruckner A., Zhang S. M., Beller M., Angewandte Chemie International Edition, 46, 8866-8868, 2007.
[18]. Bautista F. M., Campelo J. M., Luna D., Marinas J. M., Quiros R. A., Romero A. A., Applied Catalysis B: Environmental, 70, p. 611-620, 2007.
[19]. Frank J. Owens, Charles P. Poole Jr., *The Physics and Chemistry of Nanosolids*, p. 1-40, 2009.
[20]. Wu W., He Q., Jiang C., Nanoscale Res Lett., 3:397, 2008.
[21]. ***, Nanocrystals. Nat Mater., 3:891, 2004.
[22]. Zhou Z., Zhu X., Wu Park J., An K., Hwang Y., Park J.-G., Noh H.-J., Kim J.-Y. *et al.*, Chem. Mater., 27, p. 3505-3515, 2015.
[23]. Roh Y., Vali H., Phelps T. J., Moon J. W., J Nanosci Nanotechnol, 6, p. 3517-3520, 2006.
[24]. Bharde A. A., Parikh R. Y., Baidakova M., Jouen S., Hannoyer B., Enoki T., *et al.*, Langmuir, 24, p. 5787-5794, 2008.
[25]. Aftabtalab A., Sadabadi H., Chakra C. S., Rao K. V., Sarah Shaker, Mahofa E. P., IJSER, 5, p. 1419-1423, 2014.
[26]. Massart R., 17, p. 1247-1248, 1981.
[27]. Laurent S., Forge D., Port M. Rev. Chem. Eng., 108, p. 2064-2110, 2008.
[28]. Sun S., Zeng H., J Am Chem Soc. 124, p. 8204-8205, 2002.
[29]. Kang Y. S., Risbud S., Rabolt J. F., Stroeve P. Chem., 8, p. 2209-2211, 1996.
[30]. Ahn T., Kim J. H., Yang H.-M., Lee J. W., Kim J.-D., J. Phys. Chem. C., 116, p. 6069-6076, 2012.
[31]. Lenders J. J. M., Altan C. L., Bomans P. H. H., Arakaki A., Bucak S., de With G. Sommerdijk, N.A.J.M., 14, p. 5561-5568, 2014.
[32]. Abdelmajid L., Brahim D., Abdellatif G., Salah A., Results in Physics, 7, p. 3007-3015, 2017.
[33]. Khalil M. I., Arab J. Chem., 8, p. 279-284, 2015.
[32]. Rockenberger J., Scher E. C., Alivisatos A. P., J. Am. Chem. Soc., 121, p. 11595-11596, 1999.
[33]. Park J., An K., Hwang Y., Park J. G., Noh H. J., Kim J. Y., Park J. H., Nat. Mater., 3, p. 891-895, 2004.
[34]. Maity D., Choo S.-G., Yi J., Magn Magn Mater., 32, p. 1256-1259, 2009.
[35]. Yu W. W., Falkner J. C., Yavuz C. T., Colvin V. L., Chem. Commun, p. 2306-2307, 2004.
[36]. Sun S., Zeng H., J. Am. Chem. Soc., 124, 8204, 2000.
[37]. Cui H., Liu Y., Ren W., Adv. Powder Technol., 24, p. 93-97, 2013.
[38]. Bilecka I., Djerdj I., Niederberger M., Chem Commun., p. 886-888, 2008.
[39]. Vijayakumar R., Koltypin Y., Felner I., Gedanken A., Mater. Sci. Eng., 286, p. 101-105, 2000.
[40]. Amir Hassanjani-Roshana, Mohammad Reza Vaezi, Ali Shokuhfar, Zohreh Rajabali, Particuology, 9, p. 95-99, 2011.
[41]. Azadeh A., Mojtaba B., Morsali A., J Exp Nanosci, 6, p. 217-225, 2011.

THE ANNALS OF "DUNAREA DE JOS" UNIVERSITY OF GALATI
FASCICLE IX. METALLURGY AND MATERIALS SCIENCE
N°. 3 - 2019, ISSN 2668-4748; e-ISSN 2668-4756
Article DOI: https://doi.org/10.35219/mms.2019.3.05

OPTIMIZING THE TAKING OF THE SAMPLES FROM THE CONTAMINATED SITES WITH THE AID OF THE DRONES

Dorin EFTIMIE
"Dunarea de Jos" University of Galati, Romania
e-mail: dorin.eftimie@ugal.ro

ABSTRACT

Monitoring environmental parameters as well as taking samples from contaminated sites using drones is an optimized solution to transmit real-time minimum in-flight data on samples taken.

3D modeling using NX 8.0 software allowed the modular construction of experimental drone.

The following monitoring tests were performed with the help of the experimental drone:

• video testing of an area on the Braila-Galati dam and capturing the images on digital memory storage.

• collection of samples from water as well as depth measurements.

• monitoring the quality of the air as well as the quantity of pollution in urban traffic at a crossroad in the city of Braila.

The drone can be an efficient solution for taking samples from contaminated sites depending on the equipment with which it is equipped.

KEYWORDS: Drone, 3D model, monitoring sites environment parameters

1. Overview

Monitoring of environmental parameters may be done with the help of drones.

The technology has developed very rapidly and new, more efficient monitoring methods and reduced costs for timely information collection and communication have emerged.

2. Drone 3D modeling and the model

In Figure 1 is shown the 3D modelling of the drone with software NX 8.0 from Siemens. The 3D modelling allowed virtual verification of the correctness of the design [1].

In Figure 2 is shown the drone model and all its components [2].

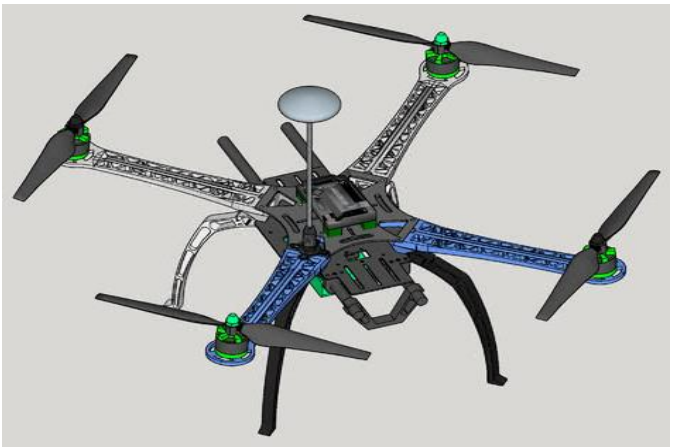

Fig. 1. *"3D" modeling of the drone*

THE ANNALS OF "DUNAREA DE JOS" UNIVERSITY OF GALATI
FASCICLE IX. METALLURGY AND MATERIALS SCIENCE
Nº. 3 - 2019, ISSN 2668-4748; e-ISSN 2668-4756
Article DOI: https://doi.org/10.35219/mms.2019.3.05

Fig. 2. *Drone frame*

3. Monitoring of environmental parameters in contaminated sites with the help of drones

The novelty of the technology developed within the project is the attempt to solve this lack of an intermediate resolution level by using the following methods of investigation:

- medium and low altitude aerial exploration performed using ground-based multi-rotor flight platforms;
- complex image processing with the help of advanced techniques in the field;
- digital models of high-resolution terrain;
- the extensive use of the most efficient techniques of geophysical investigation.

Fig. 3. *Video testing on Braila-Galati dam*

In the study of the monitoring of environmental parameters we used the drone together with a variety of sensors placed on different areas of the drone, which can perform a variety of monitoring tasks.

Ultrasonic sensors with a frequency of 44 KHz were used to perform the acoustic monitoring, allowing them to record fine sounds.

In Figures 3 and 4 are video images taken from the Braila-Galati dam area, high resolution images that can show aspects needed for experimental research.

Fig. 4. *Video testing on Braila-Galati dam*

The digital camera allows video recording and image capture on a digital storage memory.

The digital camera of the drone has the following specifications:

• Sensor 12 Mega Pixel;

THE ANNALS OF "DUNAREA DE JOS" UNIVERSITY OF GALATI
FASCICLE IX. METALLURGY AND MATERIALS SCIENCE
Nº. 3 - 2019, ISSN 2668-4748; e-ISSN 2668-4756
Article DOI: https://doi.org/10.35219/mms.2019.3.05

- 1.5-inch LCD display;
- Fast image processor;
- Photo resolution 12 sqm;
- HD video resolution 1920 x 1080/30 frames per second;
- 900 mAh removable battery;
- Dimensions 29.8 x 59.2 x 41 mm;
- Weight with battery 44 g;
- Weight without battery 58 g.

In Figure 5 is shown how depth measurements were performed and water samples were collected in August of 2019.

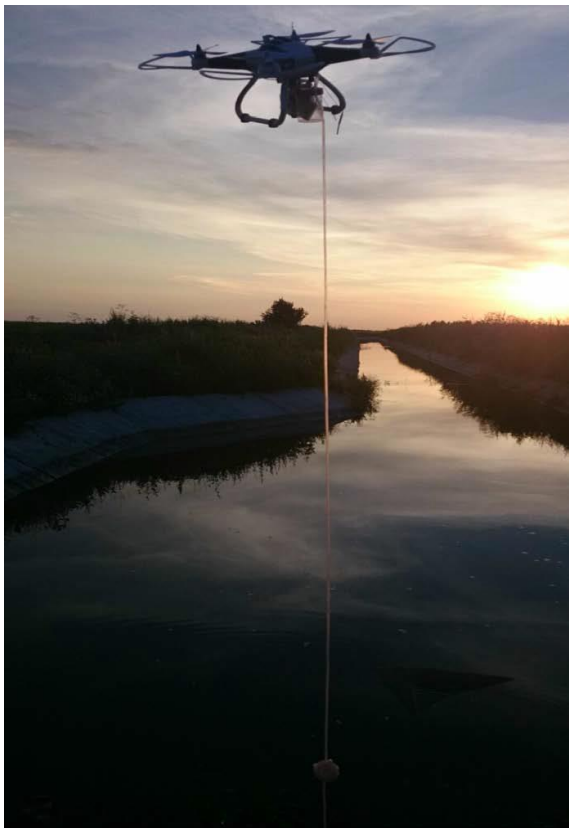

Fig. 5. *Collecting water evidence*

The determinations made in the laboratory of the water samples taken are presented in Table 1.

Liquid sampling was performed using the complex water extraction system. The following components have been fitted to perform the extraction of liquids from hard-to-reach areas:

- hose 3 m long;
- mini pump with electric drive;
- liquid sensor.

Laboratory measurements show small exceeding of the maximum allowed values

In Figure 6 is shown how were made determinations regarding the monitoring of the noxious at the crossroad between Călărași street and Griviței street in Brăila in 2019 (Table 2).

The values obtained were processed in laboratory and there are close to maximum values allowed.

Table 1. *The values obtained from the collected samples*

	pH	Dry filterable residue 105 ºC mg/dm^3	Total Fe (Fe^{3+}) mg/dm^3	Nitrates (NO_3^-) mg/dm^3
Normal values	8.5	1000	1	30
Obtain values	8.6	1100	0.9	35

Fig. 6. *Determination of traffic noxious*

Table 2. *Values obtained from research on pollution from intersections*

Month	CO µg/m^3	NO_2 µg/m^3	SO_2 µg/m^3
Maximum allowed values	15	0.1	0.2
January	9	0.03	0.1
May	11	0.06	0.15
August	13	0.08	0.2

With the help of the sensor attached to the drone, the quality of the air and the quantity of the noises can be monitored, and the drone will transmit in real time the values obtained with the help of his sensor to the base.

THE ANNALS OF "DUNAREA DE JOS" UNIVERSITY OF GALATI
FASCICLE IX. METALLURGY AND MATERIALS SCIENCE
Nº. 3 - 2019, ISSN 2668-4748; e-ISSN 2668-4756
Article DOI: https://doi.org/10.35219/mms.2019.3.05

By building the drone and equipped with last generation technology, it was able to monitor and take samples under optimum conditions and could transmit real-time minimum in-flight data on samples taken.

The drone comes with state-of-the-art technology, namely a small, ultra-powerful Chip that allows the drone to capture high quality images and videos. Subsequently, the artificial intelligence system with which the drone is equipped, serves to detect, recognize and learn the scenarios of everyday life. Drone is a first in the industry, when advanced visual guidance systems were introduced as standard functionality. The product finds its applicability both industrially and commercially.

The culture monitoring is performed by a 3D camera with a very high-performance technology, this having the performance to be able to create a 3D map in real time to monitor the state of the soil / agriculture

Soil temperature monitoring: Drones with multispectral or thermal sensors can identify dry areas or flooded areas, being able to transmit the situation in real time to make a quick decision in saving the crop.

The sampling of water from water ponds is a dangerous activity, with a high degree of risk, usually carried out by the environmental personnel at the active places, developing a more innovative process for collecting water samples from flooded ponds, settling ponds, evaporation ponds and other bodies of water, safe from the dangerous risks associated with this task.

4. Conclusions

The technology has developed very rapidly and new, more efficient monitoring methods and reduced costs for timely information collection and communication have emerged.

Drones come with state-of-the-art technology, namely a small, ultra-high-performance Chip that allows drones to capture high-quality images and videos.

The drone is a first in the industry, being for the first time introduced advanced visual guidance systems as standard functionality. The product finds its applicability both industrially and commercially.

With the help of drones, we can get high resolution photos and videos, with the help of the remote accessed camera we can get a very clear image enlargement. Scientists dealing with volcanic eruptions study from a distance, using drone imaging technology to check the trajectory of the ash thrown. Sometimes scientists even engage in risky missions to collect evidence using drones from cracks created by earthquakes.

References

[1]. ***, *High-End solution CAD/CAM/CAE Siemens NX 8.0*.
[2]. ***, http://www.digitaltrends.com/cool-tech/google-joins-nasa-and-others-to-work-on-drone-traffic-control-system/.

THE ANNALS OF "DUNAREA DE JOS" UNIVERSITY OF GALATI
FASCICLE IX. METALLURGY AND MATERIALS SCIENCE
Nº. 3 - 2019, ISSN 2668-4748; e-ISSN 2668-4756
Article DOI: https://doi.org/10.35219/mms.2019.3.06

3D MODELING OF RECYCLING EQUIPMENT BY MAGNETIC SEPARATION OF USED SANDBLASTING SAND

Dorin EFTIMIE
"Dunarea de Jos" University of Galati, Romania
e-mail: dorin.eftimie@ugal.ro

ABSTRACT

The paper presents the 3D modelling of recycling equipment by magnetic separation of the used sandblasting sand. The modelling was done using the software NX 7.5 from Siemens.

Magnetic separation is performed in three stages, two steps in dry separation and one step in wet separation. The magnetic separation operation is performed with three drums with remnant magnets designed optimized according to the design requirements.

3D modelling of this type of equipment will allow modular design for any parameters required by the design theme.

KEYWORDS: recycling used sandblasting sand, 3D modelling of recycling equipment

1. Overview

Sandblasting is the process of cleaning or finishing by abrasive blasting of surfaces made of metal, stone, glass or other solid material. This is done with the help of metallic pellets, sand or other granular abrasive materials which are driven with speed by mechanical centrifugation or by a jet of gas (compressed air) or liquids (pressurized water) to the surfaces to be processed. Sandblasting is used when, in order to paint, it is necessary to clean complex metal surfaces that do not allow the use of other methods. It is executed in enclosed spaces (Fig. 1) due to the high degree of danger presented by the jet of compressed air and sand at very high speeds [1].

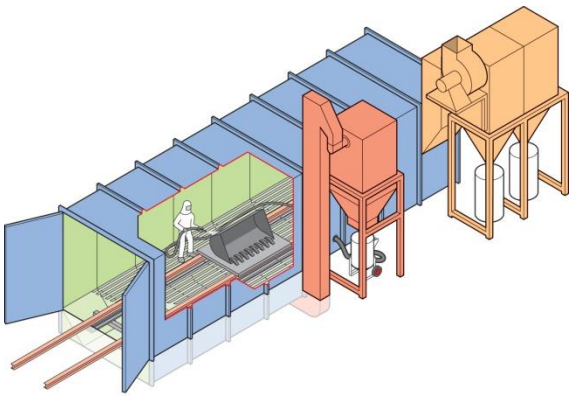

***Fig. 1.** Sandblasting chamber*

Sandblasting is used in the metallurgical industry, shipyards and generally speaking wherever rapid cleaning of surfaces is required.

The sand is used for sandblasting, because it is very cheap, but for environmental and operator protection reasons, its use has been restricted.

2. 3D modelling of recycling equipment

Figure 2 shows the principle of separation of the metal sand mixture by means of a magnetic separation system. The 3D modelling was made with NX 8.0 software of Siemens. The metal sand mixture is introduced into the bowl. Using a conveyor belt, it is transported to the magnetic separator. The magnetic separator with three magnet drums separates the metal sand. As shown in Figure 2 the drums have the opposite direction of the clockwise. The first separation that takes place in the first drum is a dry separation. After the mixture passes through the first drum, a metallic part runs on the drum and falls gravitationally into the separation of metallic particles. The second separation is made even in the second drum. The metal particles in the mixture stick to the drum and fall gravitationally into the separation of metal particles. The last drum makes a wet magnetic separation. Sand and water enter into fine sites where the water separates from the sand. The water is transported by means of pumps to a filtration unit, which is then fed back into the system.

THE ANNALS OF "DUNAREA DE JOS" UNIVERSITY OF GALATI
FASCICLE IX. METALLURGY AND MATERIALS SCIENCE
N°. 3 - 2019, ISSN 2668-4748; e-ISSN 2668-4756
Article DOI: https://doi.org/10.35219/mms.2019.3.06

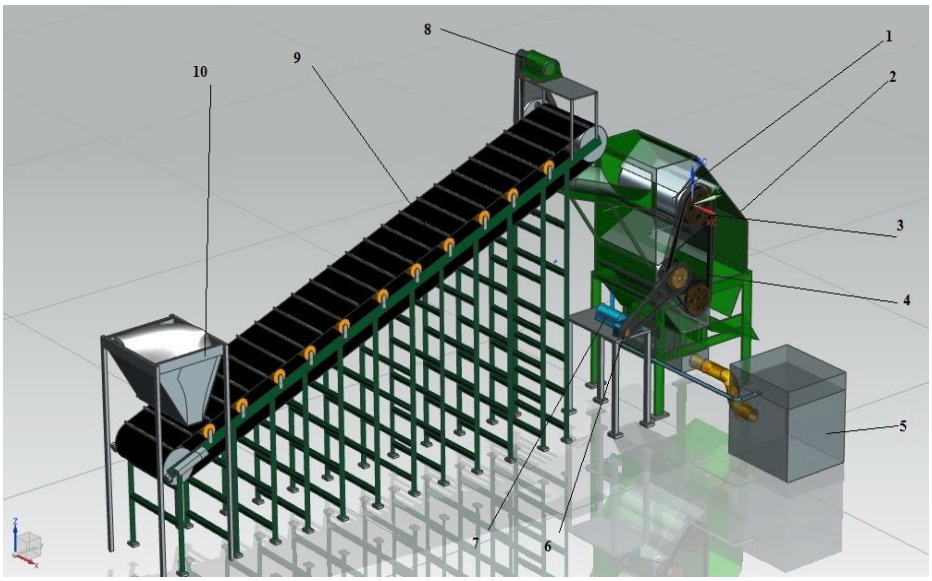

Fig. 2. *The general assembly of the magnetic separation system of the sandblasted sand 1 - Drum with permanent magnets, 2 - framework of the magnet separator, 3 - belt drive, 4 - belt, 5 - water purification unit, 6 - reducer, 7 - electric motor for driving the drums, 8 - electric motor for driving the conveyor belt with rake, 9 - conveyor belt with racks, 10 - tank with sandblasted sand*

The first subassembly that was brought in the working window is the conveyor belt with racks. As shown in Figure 2, the conveyor belt is composed of the fixed frame which the rollers are mounted. The tape is made of a rubber material and is driven by two drums, the driving drum and the driven drum. The driving drum is driven by an electric motor with variable speed. The speed of the driving drum must be correlated with the speed of the magnetic separation drums. The transmission ratio from the electric motor shaft to the drive drum drive wheel is 1:5. The driven drum slides on a rail to extend the conveyor belt with two tension straps.

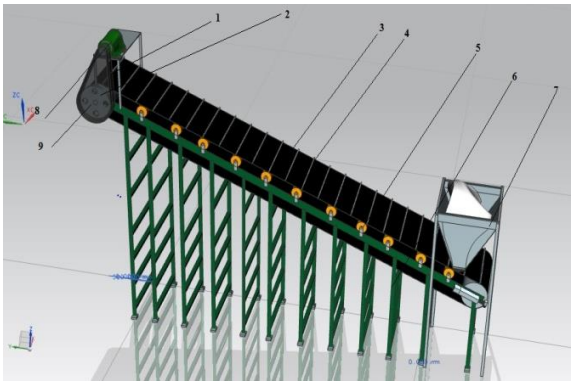

Fig. 3. *Conveyor belt with racks 1 - drive belt, 2 - drive drum wheel, 3 - belt, 4 - rake, 5 - roller, 6 - rigid metal frame, 7 - tank, 8 - electric drum drive motor, 9 - belt guard*

In Figure 3 you can see the conveyor belt with the main components that compose it.

The magnetic separator is the most important subassembly in the magnetic separation system. This can be seen in Figure 4. As seen, it is driven by an electric motor. The speed of magnetic separation drums is reduced by means of a reducer.

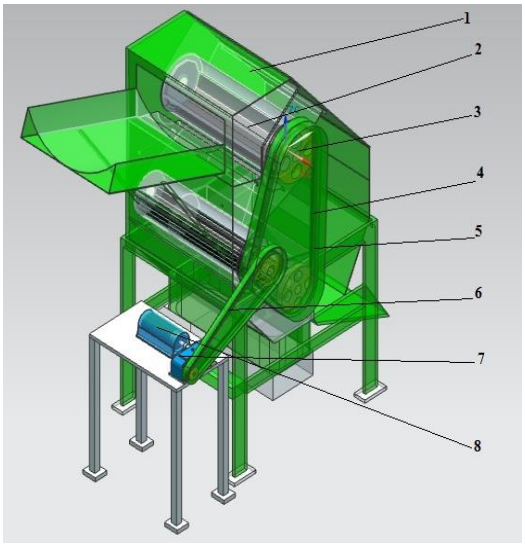

Fig. 4. *Magnetic separator 1 - Framework, 2 - magnetic drum, 3 - belt wheel, 4 - belt guard, 5 - drum drive belt, 6- reducer drive belt- magnetic separator, 7- reducer, 8- magnetic separator drive motor*

THE ANNALS OF "DUNAREA DE JOS" UNIVERSITY OF GALATI
FASCICLE IX. METALLURGY AND MATERIALS SCIENCE
Nº. 3 - 2019, ISSN 2668-4748; e-ISSN 2668-4756
Article DOI: https://doi.org/10.35219/mms.2019.3.06

As shown in Figure 5, the magnetic separator with permanent magnets has three magnetic reels which are driven by a wide belt. The last drum of the magnetic separator is sprinkled with a splash. The sprinkler is a pipe with a diameter of mm = 20 mm and has holes of 5 mm in diameter, positioned at distances equal to 20 mm. The last drum performs a wet separation. The sprinkler can be seen in figure 3, where we have a longitudinal section of the magnetic separator.

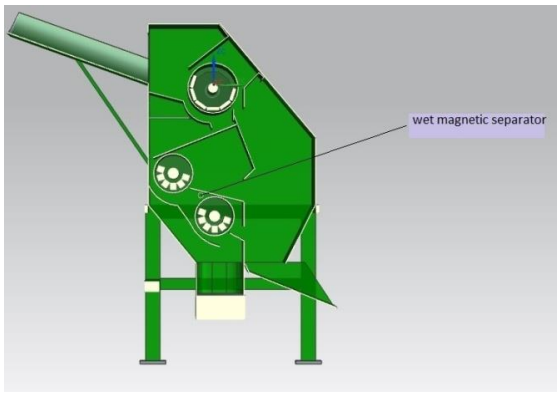

Fig. 5. *Magnetic separator section*

The main subassembly of the magnetic separator is the permanent magnet drum see Figure 6.

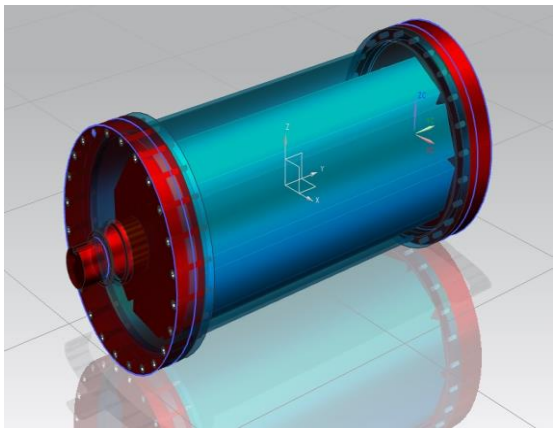

Fig. 6. *Drum with permanent magnets*

The permanent magnet drum is a subassembly made up of a plate with 2 welded shoulders (see Figure 7) at the ends to attach to two ends caps.

The cover that covers the screwed sheet is clamped with hex screws with hexagon head. The cover must be mechanically machined because it also acts as a drive shaft for the drum.

The cover can be seen in Figure 8. As seen, it is provided with a wedge channel for fastening the belt wheel.

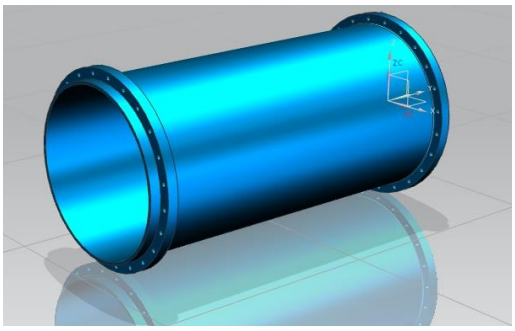

Fig. 7. *Drum housing*

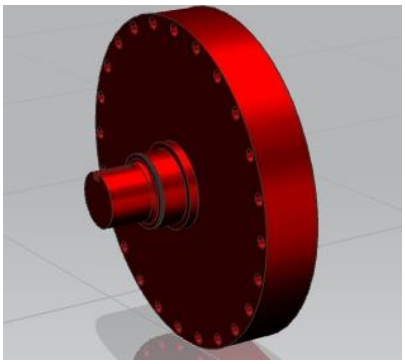

Fig. 8. *Drum cover*

Inside the drum housing there is a subassembly formed of two polygonal plates having 10 sides each and on which six permanent magnets are glued. Polygonal plates are pierced by a shaft, and caught in mounting bolts by the shaft flanges. The shaft is machined at the end as it enters these two bearings with needles. A Seeger ring is provided as the end of the bearings. The arrangement of the magnets can be seen in the subassembly of Figure 9.

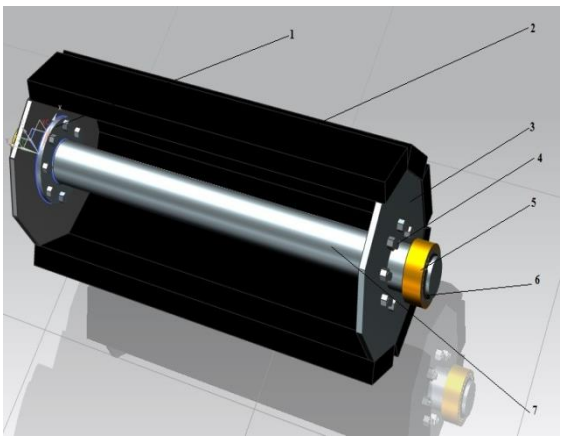

Fig. 9. *The arrangement of permanent magnets 1 - Welded flange, 2 - permanent magnets, 3 - Polygonal plate, 4 - fixing screws, 5 - needle bearing, 6 - Seeger ring, 7 - axis*

THE ANNALS OF "DUNAREA DE JOS" UNIVERSITY OF GALATI
FASCICLE IX. METALLURGY AND MATERIALS SCIENCE
Nº. 3 - 2019, ISSN 2668-4748; e-ISSN 2668-4756
Article DOI: https://doi.org/10.35219/mms.2019.3.06

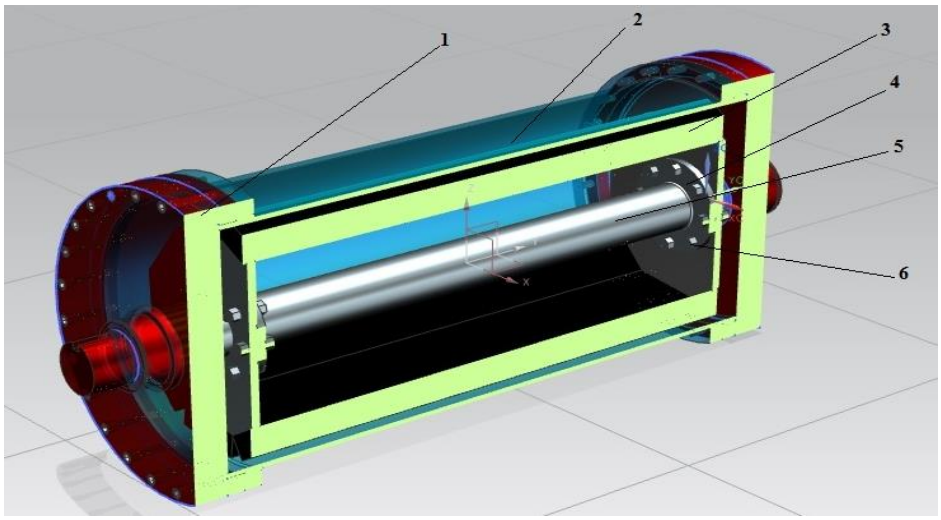

Fig. 10. *Magnetic drum section 1 - Drum cover, 2 - drum housing, 3 - magnets, 4 - welded flange, 5 - fastening screws*

The subassembly is mounted in the covers provided with mounting bearings. What is interesting about this drum is that the drum has a rotating motion, and the permanent magnets remain in a resting position. This is due to bearings that have a rolling motion and reduced friction between the cover port and the magnet axis. For a clearer image of mounting the subassembly, a section was made through it in Figure 10.

3. Conclusions

After the blasting process, the following wastes appear in the EC Framework Directive no. 75/442/EEC:

- wastes from the removal of paints and varnishes containing organic solvents or other dangerous substances;
- wastes in the form of powders in suspension which occur especially when blasting with air;
- wastes resulting from cleaning of metallic surfaces of rust and shear, especially encountered on surfaces that are painted first;
- waste resulting in the form of dust and suspensions of ferrous metals;
- waste from welding operations;
- wastes from blasting material.

The sand used in the blasting operation is found in large quantities at the shipyards and is an environmental problem. The equipment proposed in the paper represents an ecological solution within the line of recycling of the used sand used for blasting.

References

[1]. ***, https://www.worksafe.qld.gov.au
[2]. ***, High-End solution CAD/CAM/CAE Siemens NX 8.0.

THE ANNALS OF "DUNAREA DE JOS" UNIVERSITY OF GALATI
FASCICLE IX. METALLURGY AND MATERIALS SCIENCE
N°. 3 - 2019, ISSN 2668-4748; e-ISSN 2668-4756
Article DOI: https://doi.org/10.35219/mms.2019.3.07

3D MODELING AND NUMERICAL SIMULATION OF A WATER SOFTENER DEVICE

Dorin EFTIMIE
"Dunarea de Jos" University of Galati, Romania
e-mail: dorin.eftimie@ugal.ro

ABSTRACT

Water treatment in the magnetic field is not an officially recognized method of water softening. This method can be promoted as an alternative to water softening without potentially toxic chemical agents.

The water softener device consisting of 3 pairs of permanent magnets made of neodymium was designed with the help of Solid Edge software.

Numerical simulation was performed using ANSYS WORKBENCH finite element analysis software using the FluidFlow (CFX) module. With this analysis module the dynamic analysis of the fluid flow through a pipe was performed.

Three numerical analyses of the water flow through a pipe with an internal diameter of 20 mm were performed at a pressure of 2 bars, namely:

• the water flow without magnetic influences;

• the water flow under the magnetic influence of the softener device positioned longitudinally with the pipe;

• the water flow under the magnetic influence of the softener device positioned transversely with the pipe.

The conclusions of these simulations can be the basis for future research in order to optimize this type of device.

KEYWORDS: magnetic water treatment analyse, water softening, water softener device

1. Overview

Water has an essential role in life maintenance. Life could not exist without water. Every organism has water in its composition, all organs, tissues or biological fluids. Water dissolves and transports assimilated and unassimilated substances. Water keeps constant salts concentration in the body. Water takes part in temperature adjustment, evaporating on the surface of the body. In plants, water contributes to osmotic phenomena and has a great importance in the photosynthesis process.

Water has the ability to dissolve very many substances. In nature, water is not chemically pure. Natural waters contain varying amounts of substances, from gases and dissolved salts to organic substances and bacteria. Water is a vital part in many metabolic processes of the body. It is a universal solvent of living matter, being the molecular framework in which life processes are carried out.

Drinking water is that water whose quality must ensure perfect health of the end user. Coming from the natural environment, water must undergo a series of treatments that make it suitable for human consumption.

Magnetic treatment – even if this method of water treatment for softening is not officially recognized, water treatment in the magnetic field is promoted as a safe alternative of treating water with potentially toxic chemical agents.

Water treatment systems with magnetic devices are an alternative to conventional chemical or physical treatment systems and have the advantage of removing mineral and organic suspensions such as algae or microorganisms, inhibiting corrosion of pipes used for water transport and so on. When a stream of water is subjected to a magnetic field, which can be induced by an electric field or by the media of minerals, such as magnetite, polarization of the constituent minerals of the water occurs and the ionic charge changes of these minerals. The effluent of such an installation is less hard water, forming groups (the classical groups of cells of 12-18 molecules of water are divided into 6 groups, following ionization) with high hydration properties

THE ANNALS OF "DUNAREA DE JOS" UNIVERSITY OF GALATI
FASCICLE IX. METALLURGY AND MATERIALS SCIENCE
Nº. 3 - 2019, ISSN 2668-4748; e-ISSN 2668-4756
Article DOI: https://doi.org/10.35219/mms.2019.3.07

and with high penetration capabilities in the body (Fig. 1) [1].

Many such devices consist of one or more permanent magnets applied, either inside or on the outer surface of the water inlet pipe. The water is exposed to the magnetic field as it flows through the pipe between the magnets (Fig. 2) [2]. Water and water solutions passed through these magnetic fields acquire finer and more homogeneous structures. This increases the fluidity of the water and contributes to increasing the ability of the water to dissolve various constituents, such as minerals and vitamins), and therefore improves the biological activity of the solutions, which positively affects the performance of humans, animals and plants.

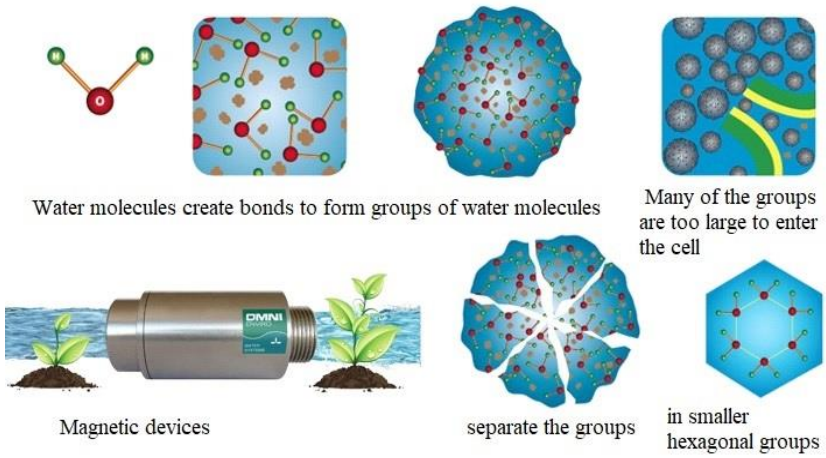

Fig. 1. *The principle of magnetic water*

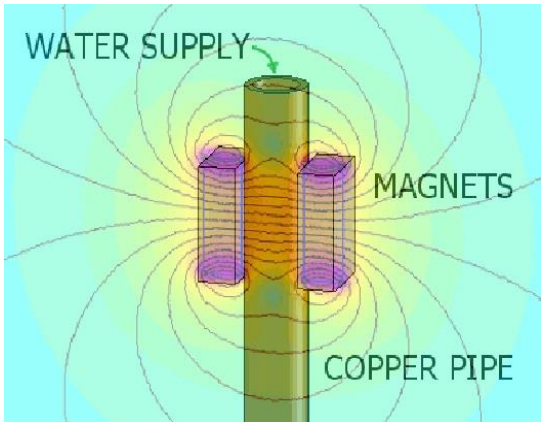

Fig. 2. *Magnetic treatment assembly*

Magnets affect the angle of connection between the hydrogen and the oxygen atom in the water molecule. The magnetization of water causes the hydrogen-oxygen bond angle in the water molecule to decrease from 104 to 103 degrees. This, in turn, causes the water molecule to gather together in groups of 6-7 molecules and not 10-12 or more (Fig. 3) [1]. Smaller groups lead to better water absorption through cell walls. Dr. Michael Lam, in his study of magnetized water, reports that there were numerous mentions of people who drank magnetized water every day who were cured of many chronic degenerative diseases, such as kidney stones and arthritis.

The theory of water magnetization is that water flows underground, comes into contact with the electromagnetic field of the earth and the magnetic charge is passed into the water. When the water is treated for drinking, it is passed through metal pipes, which demagnetize it. Magnetizing the drinking water breaks the surface tension, making it easier to absorb from every cell in the body. In addition, there is a strong side benefit. Applying a magnetic field to water can increase its pH (up to a whole point, depending on the water).

Magnetically treated water directs water through a strong magnetic field. By placing two strong neodymium magnets on each side of the inlet pipe, all the water passes through a strong, uniform magnetic field. Treating the water with magnets does not remove calcium from the water, but claims that it changes the structure of the deposits that are formed, causing them to adhere less to the surfaces.

A large variety of magnetic water treatment devices are available, but most consist of one or more permanent magnets fixed inside or on the outer surface of the water inlet pipe. The water is exposed to the magnetic field as it flows through the pipe between the magnets (Fig. 2). An alternative approach is to use the electrical current that runs through wire strands wrapped around the water pipe to generate the magnetic field.

Suppliers of magnetic water treatment devices claim that exposing water to a magnetic field will

THE ANNALS OF "DUNAREA DE JOS" UNIVERSITY OF GALATI
FASCICLE IX. METALLURGY AND MATERIALS SCIENCE
Nº. 3 - 2019, ISSN 2668-4748; e-ISSN 2668-4756
Article DOI: https://doi.org/10.35219/mms.2019.3.07

reduce the "effective" water hardness. Typical claims include the removal of limestone deposits, lower water heating bills, longer service life of water heating systems and appliances, as well as more efficient use of soaps and detergents. Thus, it is claimed that magnetic water treatment offers all the benefits of ion exchange softening.

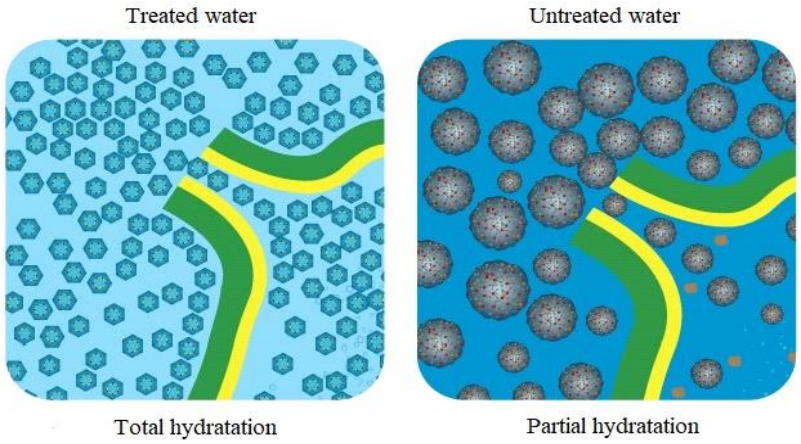

Fig. 3. *Water absorption in cells*

The "effective" hardness is claimed to be reduced by magnetic treatment. Magnesium or calcium is not removed from magnetically treated water. Instead, the claim is that the magnetic field decreases the tendency of dissolved minerals to form limestone. Even though the concentration of dissolved minerals indicates that it is still hard, the magnetically treated water is assumed to behave as softened water.

The main objectives of this paper are to demonstrate the following issues:

- reduction of the surface tension and internal water tension;
- increasing the ability of water to dissolve various substances, such as minerals from the soil;
- improving the biological activity of the solutions that positively affects the performance of the plants; generated by a water sample passed through a device for water magnetizing.

In the first phase, it is necessary to construct a device for water magnetization consisting of two metal frameworks, each one consisting of three neodymium magnets.

The device for water magnetizing has the role of magnetizing and purifying the water that passes through the magnetic field created by this device.

Practical determinations of the two samples of non-magnetized and magnetized water are performed for:

- comparison of the parameters values analysed in non-magnetized and magnetized water and evaluation of the obtained results
- evaluation of the toxic ion concentrations, respectively the elements: phenols, detergents, chloride, sulphate, boron, molybdenum, lead, cadmium, total chromium. Sometimes, even if the level of salt (chlorides) is not excessive, one or more of these elements can become toxic to plants. Many plants are particularly sensitive to boron.

Following the bibliographic studies performed, it was designed a device consisting of two metallic frameworks that have three permanent neodymium magnets each other (Tab. 1, Fig. 4).

Table 1. *Magnets properties*

Material	NdFeB
Form	Block
Dimensions	60 x 30 x 15 mm
Tolerance	+/- 0.1 mm
Nickel-plated coating	Nickel-plated (Ni-Cu-Ni)
Magnetization	N40
Attraction force	approx. 56 kg
Maximum working temperature	80 °C
Weight	210 g

Neodymium magnets are composed of iron, boron and neodymium, being ten times stronger than traditional magnets (ferrite magnets), known as the most powerful and advanced magnets in the world. Neodymium magnets are generally covered by a triple layer of Nickel-Copper-Nickel or epoxy resin offering durability and corrosion protection.

THE ANNALS OF "DUNAREA DE JOS" UNIVERSITY OF GALATI
FASCICLE IX. METALLURGY AND MATERIALS SCIENCE
N°. 3 - 2019, ISSN 2668-4748; e-ISSN 2668-4756
Article DOI: https://doi.org/10.35219/mms.2019.3.07

Fig. 4. *Permanent magnet*

The modelling of the mechanism for water magnetization was designed using the Solid Edge software.

The 3D modelling was performed also with the device positioned longitudinally (Fig. 5) and transversely (Fig. 6) in order to make a comparative analysis of the effects resulted by changing the orientation of the magnetic field.

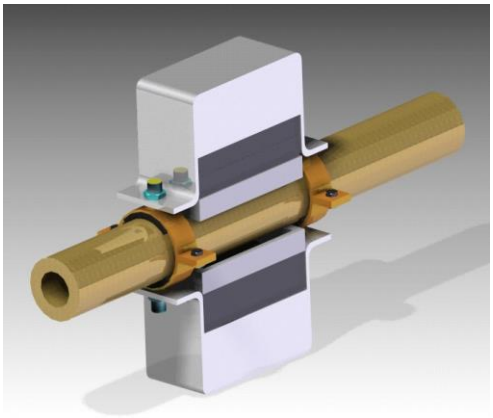

Fig. 5. *3D modelling of the device positioned longitudinally on the pipe*

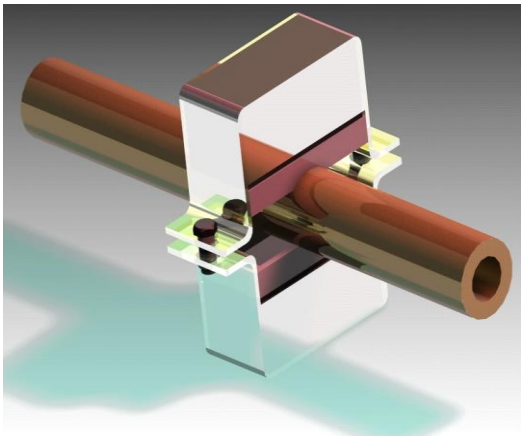

Fig. 6. *3D modelling of the device positioned transversally on the pipe*

2. Numerical simulation of the device for water magnetization

The device for water magnetizing has the role of magnetizing and purifying the water that passes through the magnetic field created by it. To demonstrate how water magnetization is performed and the effect of the magnetization device on water, a numerical simulation was performed using the ANSYS WORKBENCH finite element analysis software using the Fluid Flow (CFX) module [3]. With the help of this analysis module, dynamic analysis of fluid flow through a pipe was performed.

Three numerical analyses of water flow through a pipe were performed, namely:

- the water flow without magnetic influences;
- the water flow under the magnetic influence of the device for water magnetizing positioned longitudinally with the pipe;
- the water flow under the magnetic influence of the device for water magnetizing transversally positioned with the pipe.

It was considered that the water flows through a pipe with an internal diameter of 20 mm. The limit condition that has been applied for the water flow through the pipe is the pressure of 2 bars that is also in the current water supply systems of the houses.

The limit condition can also be seen in Figure 7.

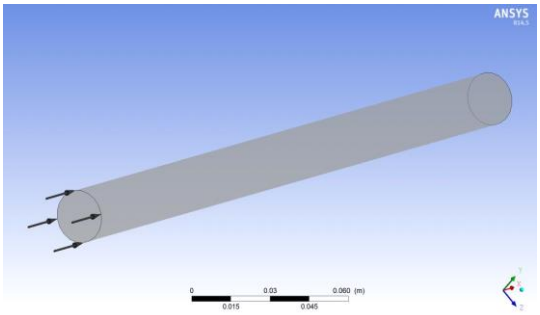

Fig. 7. *Limit conditions at the water flow through the pipe*

Following the analysis, a quasi-laminar flow was obtained.

The analysis was performed using the Fluid Flow (CFX) module in which an electro-hydrodynamic analysis was performed. The limit conditions imposed in this analysis were primarily the flow conditions of the fluid through the pipe under the pressure of 2 bars and on the other hand the magnetic intensity of the neodymium magnets inside the device.

Following the analysis, a turbulent flow was obtained due to the very strong magnetic forces acting on the flow of the fluid. The current lines resulting from this analysis can be seen in Figure 8.

THE ANNALS OF "DUNAREA DE JOS" UNIVERSITY OF GALATI
FASCICLE IX. METALLURGY AND MATERIALS SCIENCE
Nº. 3 - 2019, ISSN 2668-4748; e-ISSN 2668-4756
Article DOI: https://doi.org/10.35219/mms.2019.3.07

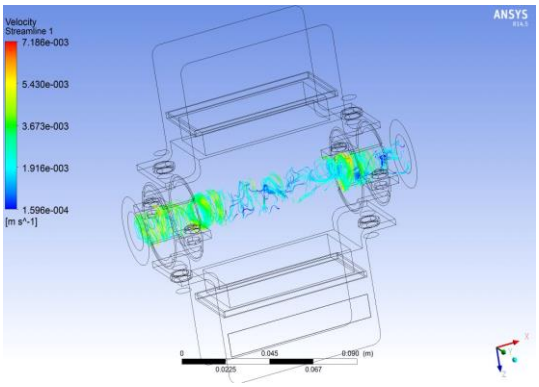

Fig. 8. *Lines of fluid flow through the pipe*

In Figure 10 can be seen how the velocity of the fluid is also influenced by the magnetic forces. In the area of magnets there is a slowdown of the fluid. This can be seen in Figure 9, how the fluid velocity at the entrance is at maximum level, highlighted by the red colour, and then decreases next to the magnets.

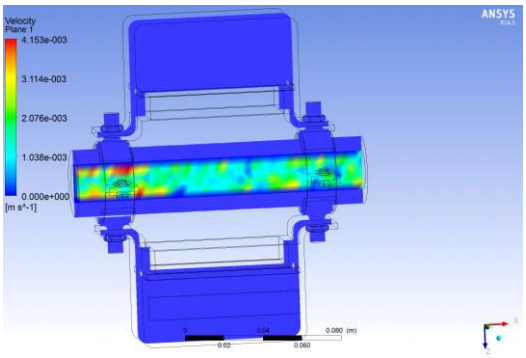

Fig. 9. *Distribution of flow velocities*

Figure 10 shows how water is magnetized with a magnetic intensity of 0.0002 T. As shown in this figure, the maximum magnetic intensity is in the center of the magnets, where the magnetic forces are also at maximum value.

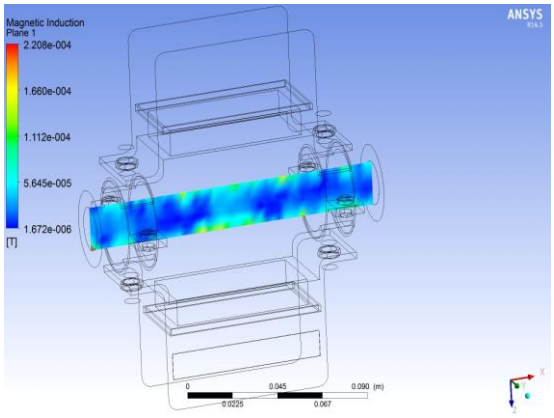

Fig. 10. *Magnetization of water*

Due to the velocity and magnetic influences the water is charged energetically with current density of $7*10^{-9}$ A/m^2. In Figure 11 you can see the energetic distribution of water. As can be seen the water is charged energetically.

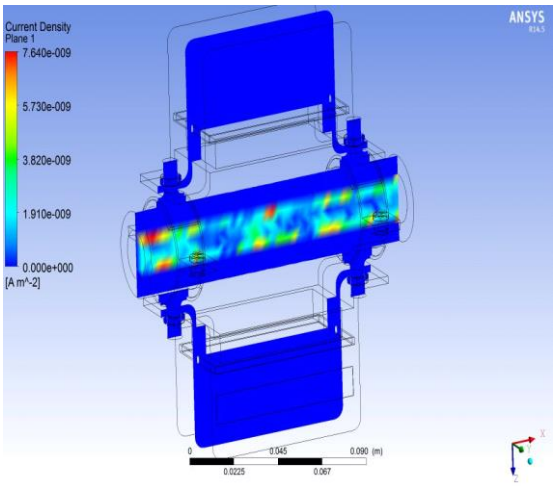

Fig. 11. *Energetic distribution of water*

In the case of the device which is transversally positioned, see Figure 12, the same limit conditions were applied as in the case of longitudinal positioning. These two analyzes that were performed, aimed at observing the efficiency of the device according to its positioning on the pipe.

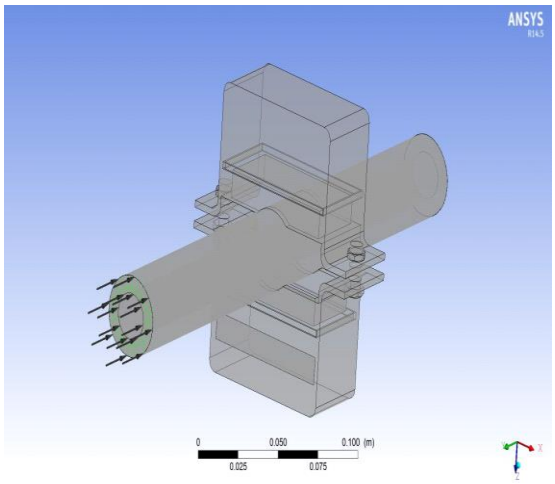

Fig. 12. *The limit conditions for the transversally positioned device*

Following the analysis, results were obtained for the flow lines, the velocities distribution, the magnetic distribution and the energetic distribution.

In Figure 13 it can be seen the flow lines in case of flow under the magnetic influence of the device positioned transversally with the pipe. As it can be

THE ANNALS OF "DUNAREA DE JOS" UNIVERSITY OF GALATI
FASCICLE IX. METALLURGY AND MATERIALS SCIENCE
N°. 3 - 2019, ISSN 2668-4748; e-ISSN 2668-4756
Article DOI: https://doi.org/10.35219/mms.2019.3.07

seen, the flow is turbulent having the maximum turbulence in the central area of the magnets where the maximum forces of magnetic influence are concentrated.

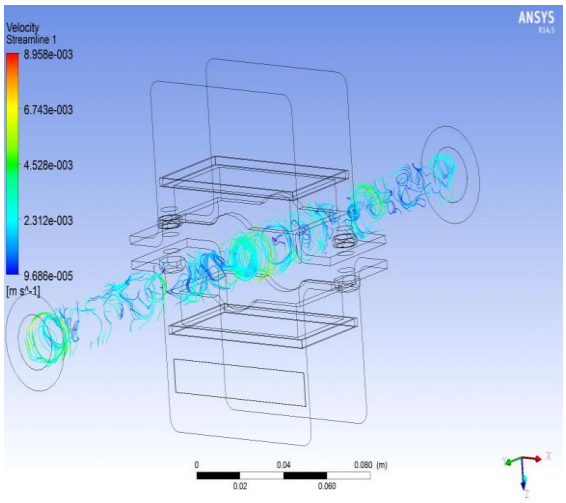

Fig. 13. *Flow lines thru pipe with transversally positioned device*

In Figure 14 can be seen a distribution of the fluid flow velocities. In this case the fluid has a higher velocity than in the first case because the area of magnetic influence is smaller than in the first case, and the magnetic forces are concentrated on a smaller portion of the pipe.

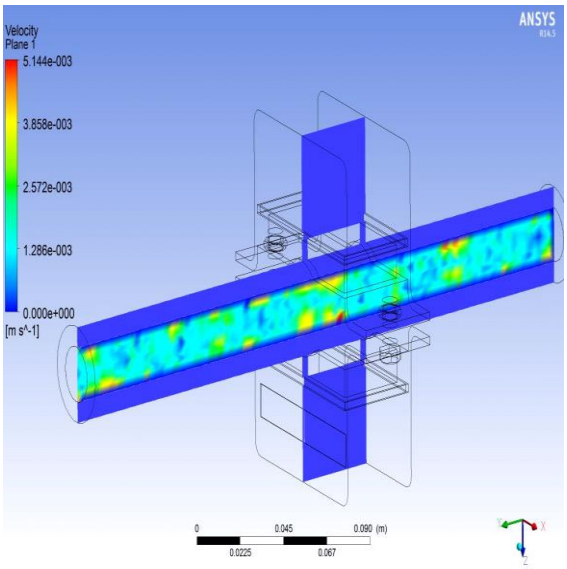

Fig. 14. *Distribution of flow velocity for the case of the transversally positioned device*

Figure 15 also shows the water magnetization distribution. In this case, the magnetic intensity of the water is lower than in the first case. The magnetization of water is twice smaller as in the case with the device positioned longitudinally along the pipe.

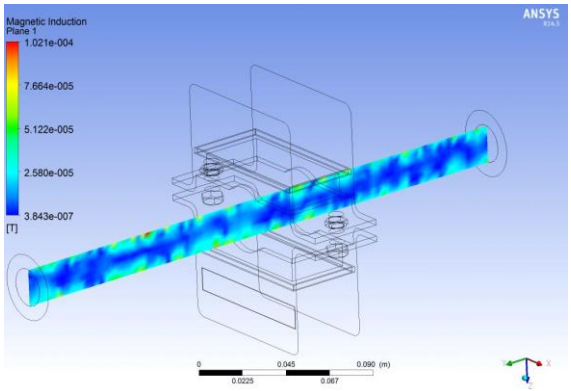

Fig. 15. *Magnetization of water with the transversally positioned device*

Lowering the magnetization of the water increases the density of the flow created because the magnetic intensity is concentrated in a smaller area than in the first case. The maximum flow density is $8x10^{-9}$ A/m^2. The energetic distribution of water can be seen in Figure 16.

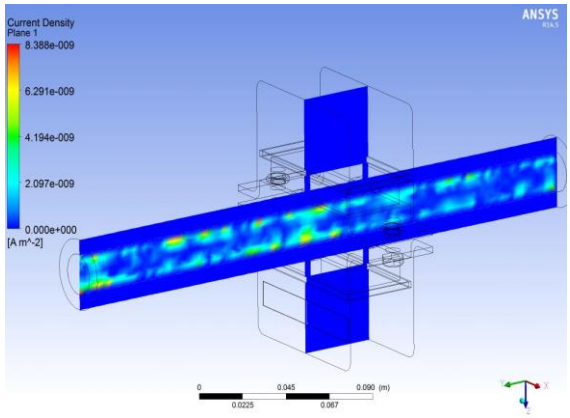

Fig. 16. *Energetic distribution of water*

3. Conclusions

Following the study there were found the following:

• the laminar flow of water is transformed into a turbulent flow under the strong influence of magnetic forces;

• the water under the strong influence of the magnetic field is magnetized;

• the flow of water through a strong magnetic field electrifies the water;

• for maximum efficiency, the proposed device for water magnetization must be positioned

THE ANNALS OF "DUNAREA DE JOS" UNIVERSITY OF GALATI
FASCICLE IX. METALLURGY AND MATERIALS SCIENCE
Nº. 3 - 2019, ISSN 2668-4748; e-ISSN 2668-4756
Article DOI: https://doi.org/10.35219/mms.2019.3.07

longitudinally on the pipe through which the water flows.

Following the numerical simulation, the variant of the device positioned longitudinally on the pipe was chosen for the construction.

References

[1]. ***, http://www.omnienviro.com/magnetized-water/.
[2]. ***, https://www.kjmagnetics.com/blog.aspp=water-treatment.
[3]. ***, https://www.ansys.com/products/fluids/ansys-cfx.

THE ANNALS OF "DUNAREA DE JOS" UNIVERSITY OF GALATI
FASCICLE IX. METALLURGY AND MATERIALS SCIENCE
Nº. 3 - 2019, ISSN 2668-4748; e-ISSN 2668-4756
Article DOI: https://doi.org/10.35219/mms.2019.3.08

INVESTIGATION OF SOME ORGANIC POLLUTANTS IMPACT ON PHYSICO-CHEMICAL CHARACTERISTICS OF PLANTLETS

Romică CREŢU
"Dunarea de Jos" University of Galati, Romania
e-mail: romy_cretu@yahoo.com

ABSTRACT

The cleaning process plays an important role in industry. On the other hand, the presence of detergents in soil can greatly impact on the environment. Therefore, the present study was conducted to evaluate the impact of two complex pollutants on some plantlets, e.g. Phaseolus vulgaris and Petroselinum crispum. In this context, this article uses various physico-chemical methods to compare the impact of non-biodegradable liquid detergent (a mixture of different compounds which contain isothiazolinone, methylisothiazolinone and 2-bromo-2-nitropropane-1,3-diol) on the environment with the one based on biodegradable origin (without 2-bromo-2-nitropropane-1,3-diol). Moreover, additional investigations showed the significant decrease in total carotenoids content and colour parameters with pollutant concentrations (0.125÷0.5%). Based on the results from the analysis performed in this paper, the contamination of soil with liquid detergents can have adverse effects on plants metabolism with plantlets height and number of leaves variation. Although there is no very strict correlation between the biometrical parameters and the concentration of the detergents used in this study, as a result of the individual enzymatic response of the plantlets to the aggression of the detergents, it is obvious that the plantlets' metabolism is negatively influenced by the presence of both detergents. Also, the content of carotenoids and xanthophylls decreased in the case of studied samples, at the highest concentration (0.5%) of non-biodegradable detergent (Phaseolus vulgaris samples) and lower concentration (0.125%) of biodegradable detergent (Petroselinum crispum samples).

KEYWORDS: biodegradable, without environmental compatibility, biometrical parameters, carotenoids and xanthophylls, colour

1. Introduction

The anthropic pollution by various activities in industry or transport has been amplified in the last decades as compared to the natural pollution, whose effects are minimal. Some pollutants may accumulate in organisms producing the phenomenon of biological amplification [1].

The cleaning process plays an important role in industry [2]. On the other hand, according to Uzma *et al.* [3] the presence of detergents in soil and water (where they can be found accidentally) can greatly impact on the environment. According to [4], it is compulsory to check the quality of the soils. Considering the possibility of some pollutants to exist in the soil, it is important to analyse them and to inform the users.

Many of the chemical substances present in the used detergent products on plantlets, e.g. common beans (*Phaseolus vulgaris*) and the parsley (*Petroselinum crispum*) are characterised by a certain degree of toxicity. Thus, the impact of used liquid detergents on plants is a complex problem. The origin of the grown species is the spontaneous parsley (*Petroselinum crispum sylvestre*), widely spread around the Mediterranean. Parsley is an allogamous plant, which means the pollination is done indirectly by insects [5].

This study focuses on specific modifications of the physico-chemical characteristics of some plantlets, e.g. *Phaseolus vulgaris* and *Petroselinum crispum*, induced by used detergents present in the soil, both bio-based and without environmental compatibility. The contents in chlorophyll (total chlorophyll) and carotenoids, known as bio-indicators

THE ANNALS OF "DUNAREA DE JOS" UNIVERSITY OF GALATI
FASCICLE IX. METALLURGY AND MATERIALS SCIENCE
N°. 3 - 2019, ISSN 2668-4748; e-ISSN 2668-4756
Article DOI: https://doi.org/10.35219/mms.2019.3.08

to monitor a variety of contaminants in the ecosystem [6] will also be evaluated.

2. Experimental Details

2.1. Plant material

The subjects were selected, after a previous documentation, on the basis of their growth and development characteristics [5]. The plantlets were grown in a "green-laboratory" at "Dunarea de Jos" University of Galati, Romania. The germination of the beans (indirect light coming from a window facing north) was monitored for 21 days, the conditions of the experiment being preserved till the moment when the plant reached the necessary stage of development to be harvested and planted into new recipients with fertile soil.

2.2. Detergents

The biodegradable detergents (which were purchased in local supermarkets from Galati, Romania) are non-toxic for the environment and do not contain phosphates, perfumes or synthetic dyes.

In order to study the impact of detergents upon the plants we used various concentrations of detergents, keeping in mind the recommendations of the producers regarding their use.

2.3. Weight ratio of chlorophylls and carotenoid analyses

Chlorophyll content was determined according to Lichtenthaler and Buschmann [7] with some modifications. The pigments were extracted in 80% acetone three times for 90 min extraction time and 1 min homogenization time. After this process for the optimization of the extractions, ultrasonication was used for 3 min. Then the samples were taken and underwent centrifugation (4000 x g, 10 min, refrigerated at 4 °C) to separate cells from solvent using a Hettich Universal 320 centrifuge. Then the solution/supernatant was used for detection of chlorophyll content by UV–Vis spectrophotometry (UV-Vis Double Beam PC 8 Auto Scanning cell UVD-3200, Lobomed, INC.) at the maximum absorption wavelengths for chlorophylls a and b, respectively [8-10]. The concentration of chlorophylls and the sum of carotenoids were determined by the equation (1).

$$\begin{aligned} c_a\ (\mu g/mL) &= 12.25 \cdot A_{663.2} - 2.79 \cdot A_{646.8} \\ c_b\ (\mu g/mL) &= 21.50 \cdot A_{646.8} - 5.10 \cdot A_{663.2} \\ c_{x+c}\ (\mu g/mL) &= (1000 \cdot A_{470} - 1.82\ c_a - 82.02\ c_b)/198 \end{aligned} \quad (1)$$

where c_a = chlorophyll *a*; c_b = chlorophyll *b*; c_{x+c} = carotenoids, Aλ = absorbance at λ (nm). The pigment concentrations are given in µg/mL extract solution.

2.4. Determination of the colour stability

Colour stability was determined using the colour coordinates which were computed in the CIELAB system in a CIE D 65/10° observer conditions [11]. The results were expressed as trichromatic parameters.

3. Experimental results

The studied plantlets with and without added detergents in topsoil with different detergent concentration were cultivated and some physico-chemical parameters were determined. When the plants reached the development stage and they could be harvested and replanted, they were transferred into recipients with fertile soil employing 180 mL single-use plastic beakers, where 50 g of flower soil had been introduced.

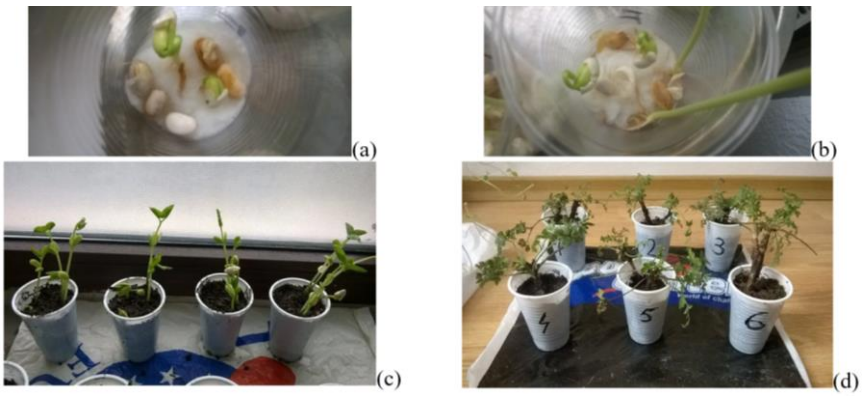

Fig. 1. *Various stages of development during germination (a) and (b) for Phaseolus vulgaris. Phaseolus vulgaris offshoots an early stage (c). Petroselinum crispum plantlets an early stage (d)*

THE ANNALS OF "DUNAREA DE JOS" UNIVERSITY OF GALATI
FASCICLE IX. METALLURGY AND MATERIALS SCIENCE
N°. 3 - 2019, ISSN 2668-4748; e-ISSN 2668-4756
Article DOI: https://doi.org/10.35219/mms.2019.3.08

The *Phaseolus vulgaris* plantlets were studied under laboratory conditions identical to those used in the case of *Petroselinum crispum* (Figure 1).

3.1. Biometric parameters analysis

During the study, the plantlets were observed in their first stage of vegetative development through the analysis of certain biometrical parameters such as: high development and the number of leaves as well as colour changes or various irregularities that appeared during the experiment. On the basis of the results obtained, the 6 samples of Phaseolus vulgaris placed under scrutiny (3 plantlets under the effect of the bio detergent, 3 plantlets under the effect of the environment incompatible detergent) displayed heights between 26 and 40 cm. Interestingly, for the duration of the experiments (14 days of detergent treatment), the impact of the liquid detergents upon the plantlets studied at their incipient stage indicated that the heights of the Phaseolus vulgaris plantlets remain constant only when using the non-biodegradable detergent in concentration of 0.125%. This indicates the fact that the presence of the detergent induces a totally inhibiting effect upon the plantlets' growth. In the other cases, a more or less significant growth in the plantlets' height was recorded (Figure 2).

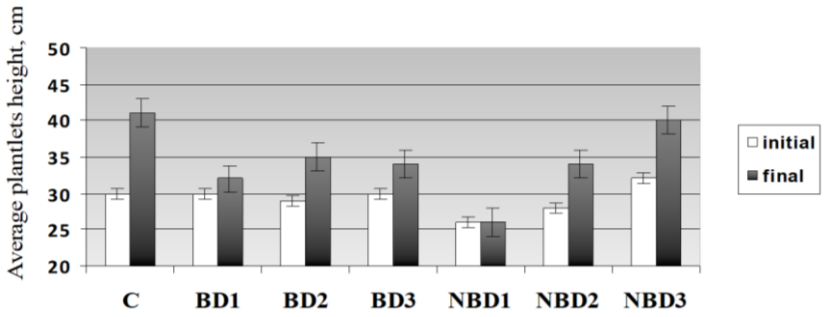

Fig. 2. *The effect of detergents (different concentrations: BD1 - biodegradable liquid detergent 0.125%, BD2 - biodegradable liquid detergent 0.25%, BD3 - biodegradable liquid detergent 0.5% and NBD1 - non - biodegradable liquid detergent 0.125%, NBD2 - non - biodegradable liquid detergent 0.25%, NBD3 - non - biodegradable liquid detergent 0.5%; C – control sample, without detergent) on the total number of the plantlets height for Phaseolus vulgaris. Vertical bars represent standard deviation of the mean (n = 3)*

The data in Figure 2 show that the largest growth in height (25%) happens when using the environment incompatible detergent (which contains isothiazolinone, methylisothiazolinone and 2-bromo-2-nitropropane-1,3-diol) with the highest concentration. The same impact of detergents was also noticed in the case of the *Petroselinum crispum* species (data not shown). It is worth mentioning the fact that the growth in height of the sample plantlets was of 36.66%. It was also noticed that spreading the detergents over the soil where the two species were planted determines, in some cases, a decrease in the number of leaves as compared to the plantlets of the witness lot (Figure 3). The differences recorded between the impacts of the two types of detergent are significant for *Phaseolus vulgaris*.

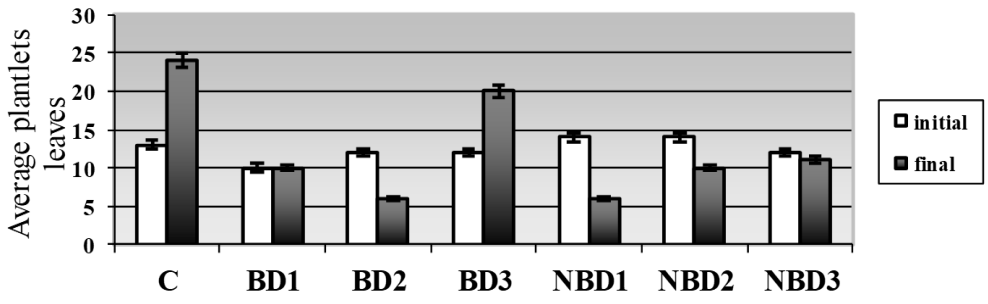

(a)

THE ANNALS OF "DUNAREA DE JOS" UNIVERSITY OF GALATI
FASCICLE IX. METALLURGY AND MATERIALS SCIENCE
Nº. 3 - 2019, ISSN 2668-4748; e-ISSN 2668-4756
Article DOI: https://doi.org/10.35219/mms.2019.3.08

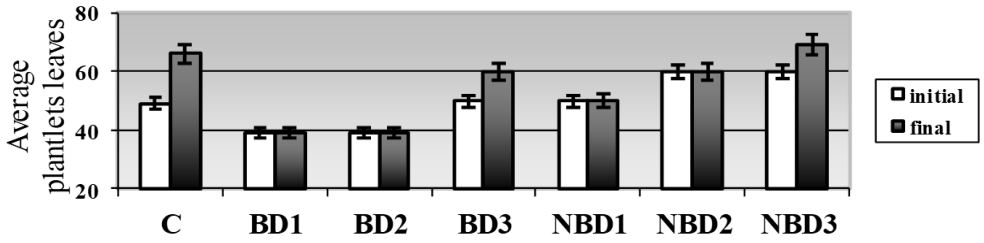

(b)

Fig. 3. *The effect of detergents on the total number of the plantlets leaves for Phaseolus vulgaris (a) and Petroselinum crispum (b). The legend as explained in Fig. 2*

After analyzing the data in Figure 3, one can see that this biometric parameter depends decisively on the interaction between the species of the plantlet and the type of detergent. Thus, although the number of leaves of the *Phaseolus vulgaris* lot placed under scrutiny was sometimes larger than that of the witness lot, the differences that appear depend on the type of detergent. There was a significant inhibition of the leaf number multiplication in the case of all samples when using non-biodegradable detergent. Moreover, the results show that whenever they get into contact with this type of detergent, the plants lose leaves no matter what concentration of detergent was used.

The highest growth in the number of leaves (20%) happens in the presence of the biodegradable detergent with the highest concentration, although it is lower as compared to the concentration of the witness sample (35% approximately) as a consequence of the impact the detergent has upon the plantlets metabolism. However, the values corresponding to the biodegradable detergents (0.125% and 0.25%) shown in Figure 3 (b) suggest a significant homogeneity regarding the leaf number of the *Petroselinum crispum* in relation with the detergent concentration.

Despite the fact that there is no very strict correlation between the biometrical parameters and the concentration of the detergents used in this study, as a result of the individual enzymatic response of the plantlets to the aggression of the detergents, it is obvious that the plantlets metabolism is negatively influenced by the presence of both detergents.

3.2. Weight ratio of chlorophylls and total carotenoids analysis

The same results were obtained in the case of samples treated with non-degradable detergent. Knowing from the specialized literature that the carotenoid pigments play a significant part in photosynthesis [12], I may assume, as in the case of chlorophyll, that certain organic substances from the composition of detergents interfere with the carotenoids' action mechanism. Moreover, the photosynthesis provides carbohydrate for plant growth [13].

The ratio between chlorophyll *a* and chlorophyll *b* is an indicator of how the photosynthesis process unfolds.

Table 1. *The weight ratio of Chls a and b to total carotenoids, (a+b)/(x+c) in the case of Phaseolus vulgaris. Abbreviations: (a + b) represent the total chlorophylls a and b; (x + c, xanthophylls and carotenes (total carotenoids)*

Detergent type	*Control sample*	*Detergent application concentration (%)*		
		0.125	*0.25*	*0.5*
BD	*4.265*	*2.274*	*2.113*	*3.094*
NBD		*2.001*	*2.341*	*2.759*

Table 2. *The weight ratio of Chls a and b to total carotenoids, (a+b)/(x+c) in the case of Petroselinum crispum. Abbreviations: see Table 1*

Detergent type	*Control sample*	*Detergent application concentration (%)*		
		0.125	*0.25*	*0.5*
BD	*5.114*	*5.111*	*4.095*	*5.079*
NBD		*2.156*	*3.258*	*4.021*

Moreover, the ratio between the quantities of chlorophyll *a* and chlorophyll *b* (Chls *a* and *b*) is an indicator of the optimum functionality of photosynthesis, as well as of the adaptation to the

THE ANNALS OF "DUNAREA DE JOS" UNIVERSITY OF GALATI
FASCICLE IX. METALLURGY AND MATERIALS SCIENCE
N°. 3 - 2019, ISSN 2668-4748; e-ISSN 2668-4756
Article DOI: https://doi.org/10.35219/mms.2019.3.08

action of certain harmful factors. The ratio between the quantities of chlorophyll *a* and *b* and the total quantity of carotenoid (xanthophylls and carotenoids), respectively (a+b)/(x+c), is an indicator of how vigorous the plant is. Usually, the (a+b)(x+c) ratio has values between 4.2 and 5 for the plants and leaves constantly exposed to sun light and values between 5.5 and 7.0 for plants and leaves exposed to shadow. Generally, the decrease of the value of the (a+b)(x+c) ratio is an indicator of stress and disturbance of the photosynthesis process in the plantlets, which can be expressed by a sudden collapse in the production of chlorophyll as compared to carotenoids. Thus, the leaves become yellow-green and presents low values for the (a+b)(x+c) ratio (3.5 or even 2.5 up to 3.0) as the plant deteriorates under the impact of the aggressing factor [14]. The results of this study are similar to findings reported by Lichtenthaler and Buschmann [7]. So, the experimental data given in Tables 1 and 2 emphasize the negative impact upon the studied plants in correlation with the presence of the detergents.

It is noticeable that in both cases the (a+b)/(x+c) ratio decreases for all concentrations of detergent applied to the soil in which the plantlets developed. In both cases, the highest stress corresponds to the non-biodegradable detergent (0.125%), this one being the fastest to reach the roots of the plantlets. However, in the case of *Phaseolus vulgaris*, under the above-mentioned experimental conditions, the stress induced by the detergents is higher than in the case of *Petroselinum crispum*.

Based on the results from the analysis performed in this paper, the content of carotenoids and xanthophylls decreased less in the case of the parsley samples, at the highest concentration of detergent, both biodegradable and non-biodegradable (Figure 4-a).

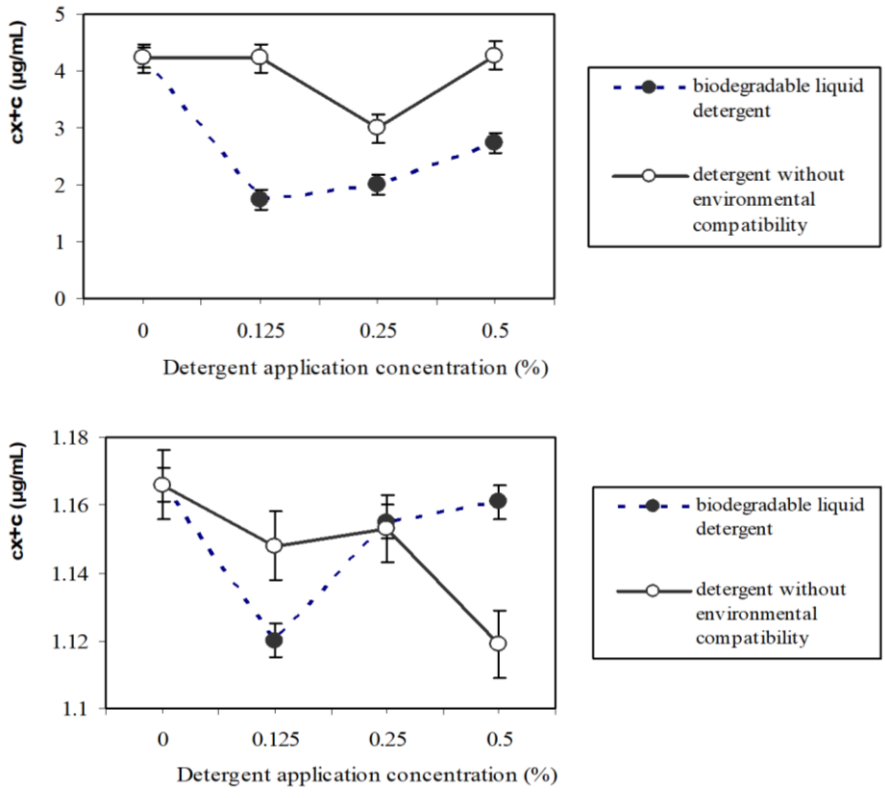

Fig. 4. *Change of the carotenoids in extracts from Petroselinum crispum (a) and Phaseolus vulgaris (b) plantlets materials treated with biodegradable detergent and detergent without environmental compatibility (see legend).* c_{x+c} *(µg/ml) represent the concentration of carotenoids (x + c = xanthophylls and carotenes)*

On the other hand, when biodegradable detergent was used, the lowest concentrations of detergent (0.125%) had the highest impact, where carotenoids and xanthophylls decreased by 58.91%.

Interestingly, in the case of the samples treated with non-biodegradable detergent, the decrease is of only 0.17%, which indicates a higher resistance of parsley to this type of detergent at this concentration. At the highest concentrations (0.5%), carotenoids and

THE ANNALS OF "DUNAREA DE JOS" UNIVERSITY OF GALATI
FASCICLE IX. METALLURGY AND MATERIALS SCIENCE
Nº. 3 - 2019, ISSN 2668-4748; e-ISSN 2668-4756
Article DOI: https://doi.org/10.35219/mms.2019.3.08

xanthophylls decreased less, 35.5% in the case of the sample treated with biodegradable detergent and only 0.12%, in the case of the sample treated with non-biodegradable detergent. These results suggest that the biodegradable detergent has a far deeper negative impact on carotenoids and xanthophylls from the parsley samples.

Similarly, to the case of the chlorophyllous pigments from the parsley samples, the impact of the detergents upon the carotenoids and xanthophylls from the bean samples was similar only for the lowest concentration of detergent (Figure 4-b). Among the samples treated with biodegradable detergent, the highest influenced was recorded in the case of the bean sample treated with 0.125% detergent, when the content of carotenoids and xanthophylls decreased by 3.95% as compared to the witness sample. On the other hand, in the case of the sample treated with non-biodegradable detergent (0.125%), the biosynthesis of carotenoids and xanthophylls decreased only by 1.54% as compared to the witness sample. However, the bean sample treated with the highest concentration of non-biodegradable detergent (0.5%) is the most affected, the content of carotenoids and xanthophylls decreasing by 4% as compared to the witness sample. When biodegradable detergent (0.5%) was used, the decrease was of only 0.26%.

The plantlets response to the action of pollutants shows the less harmful impact of the biodegradable detergent at this concentration, under the conditions of the experiments. Similar conclusions (in the cases of detergent without environmental compatibility) were obtained by Pongooni and Sasikala [15] according to which the higher concentration of detergent is toxic to the plant growth.

Moreover, in accordance with the previous studies [16] the presence of the liquid detergents in the soil, irrespective of their type, may affect irreversibly (by changes in biochemical parameters) the plantlets developing and pollination of the *Phaseolus vulgaris* and *Petroselinum crispum* plants, given their having a direct and, respectively, indirect pollination (a possibly aggressive effect aggressive upon insects).

3.3. The color evolution in the extract

In Table 3. are presented the experimental results obtained on the localization of the extracts color in the case of parsley samples, in accordance with the CIELAB color system.

Table 3. *Chromatic characteristics (CIE D 65/10° illuminat/observer conditions) for parsley samples*

Sample	Chromatic coordinates			a^*/b^*	$(a^*/b^*)^2$	C^*_{ab}	s	h_{ab}
	L^*	a^*	b^*					
C	80.30992	-43.9832	73.80029	-0.59598	0.355187	85.91276	1.069765	120.77
NBD_1	85.91638	-33.1759	55.30182	-0.59991	0.359888	64.48979	0.750611	120.8
NBD_2	86.57334	-27.1958	52.38301	-0.51917	0.26954	59.02197	0.681757	117.29
NBD_3	82.65858	-36.0706	61.37109	-0.58775	0.345446	71.18639	0.861210	120.47
BD_1	90.13535	-27.5247	44.26251	-0.62185	0.386699	52.12273	0.578272	122
BD_2	90.51459	-25.5829	44.54163	-0.57436	0.329888	51.36575	0.567486	119.89
BD_3	86.04945	-33.2269	57.52794	-0.57758	0.333596	66.43409	0.772046	120

The experimental results highlight that in the case of the parsley samples, there is a bathochromic shift from the control sample to the sample treated with the highest concentration of detergent. More than that, the high degree of uniformity of the CIELAB color space offers the possibility of a good chromatic characterization of the samples analyzed. Thus, according to Table 1, significant differences (10.2 for BD and 6.26 for NBD sample) regarding the variation in brightness (L^*) are for 0.25% detergent concentrations. The smallest variations in brightness (5.74 for BD and 2.35 for NBD sample) were obtained for the highest concentration (0.5%) of pollutant, probably due to its slower permeation to roots (under the conditions of the experiment). Also, the parameter a* (the red degree) values being lower than those of parameter b* (the yellow degree), it is obvious that the red index tends towards subunit values. Also, in this context, the chroma (C^*_{ab}) with the lowest values was obtained for the situation when the parsley came in contact with the biodegradable detergent. This fact correlates with a lower intensity of the color of the parsley in this case.

These results expressed by the chromatic parameters highlighted above are supported by another parameters of color characterization (saturation, s and hue angle, h_{ab}). A slightly lower hue angle was observed when the parsley was treated with biodegradable detergent. Similarly, information regarding the chromatic parameters in the case of the bean samples was obtained (Table 4).

Based on the results from the analysis performed in this paper, in the bean seedlings a color closure (by decreasing the parameter L*) it is observed when non-biodegradable detergent of 0.25% concentration

THE ANNALS OF "DUNAREA DE JOS" UNIVERSITY OF GALATI
FASCICLE IX. METALLURGY AND MATERIALS SCIENCE
N°. 3 - 2019, ISSN 2668-4748; e-ISSN 2668-4756
Article DOI: https://doi.org/10.35219/mms.2019.3.08

was used. Moreover, only in the case of the NBD_1 and NBD_3 the variation of the hue angle is greater than in the previous case, respectively the parsley seedlings.

Table 4. *Chromatic characteristics (CIE D 65/10° illuminat/observer conditions) for bean samples*

Sample	Chromatic coordinates			a^*/b^*	$(a^*/b^*)^2$	C^*_{ab}	h_{ab}
	L^*	a^*	b^*				
C	90.84741	-26.6219	39.37157	-0.67617	0.457208	47.52733	124.05
NBD_1	76.31048	-16.9783	19.6419	-0.86439	0.747174	25.96281	124.07
NBD_2	93.28303	-6.48838	12.95004	-0.50103	0.251032	14.48457	116.57
NBD_3	93.30917	-11.8593	18.62118	-0.63687	0.405606	22.07695	122.49
BD_1	93.67027	-5.702	11.67083	-0.48857	0.2387	12.98927	116
BD_2	94.15993	-9.45589	17.532	-0.53935	0.290899	19.91946	118.39
BD_3	93.32179	-8.78896	15.80303	-0.55616	0.30931	18.08263	119.05

Consequently, under certain experimental conditions, many of the chemical compounds present in the composition of the detergents may allow the formation certain active binding centers, fact which suggests the possibility of reducing certain specific parameters of the plantlets in the processes of involuntary pollution of the environment.

4. Conclusions

In this work the results show that the number of leaves is an indicator which decisively depends on the interaction between the species and the detergent. It was concluded that the analysis of the biometrical parameters constitutes an aspect which determines, directly or indirectly, the resistance of the species of plantlets to the action of liquid detergents.

Ratio between the quantities of chlorophyll *a* and *b* and the total quantity of carotenoids (xanthophylls and carotenoids) is an indicator of stress and disturbance of the photosynthesis process in the case of the *bean* and *parsley* plantlets.

Moreover, additional investigations showed that the significant decrease in chlorophyll and total carotenoids content was correlated with plantlets height and number of leaves variation.

The chromatic parameters determinations revealed that the change of the color of the plantlets after the absorption of the detergent components by the roots is a dynamic process that also depends on the concentration of the detergent.

This paper is part of a continuing effort to understand the metabolic changes of plants under pollutants action.

References

[1]. Horn H. A., Bilal E., Ribeiro V. E., Trindade M. W., Baggio H., *The pollution impact on the water, soil and plant generated by foundries in Pipapora and Varzeá da Palma, Minas Gerais state, Brasil*, Carpathian J. of Earth and Env. Sc., 7, p. 211-218, 2012.

[2]. Leticia Suárez, María A. Diez, Francisco A. Riera, *Recovery of detergents in food industry: an industrial approach*, Desalination and Water Treatment, p. 1-10, 2014.

[3]. Syeda Uzma, Sarzamin Khan, Waheed Murad, Nadia Taimur, Azizullah Azizullah, *Phytotoxic effects of two commonly used laundry detergents on germination, growth, and biochemical chacacteristics of maize (Zea mazs L.) seedlings*, Environ Monit Assess, 190, 651, 2018.

[4]. Dragomir Bălănică C. M., Simionescu A. G., Bîrsan I. G., Bichescu C. I., Munteniță C., *The assessment of using the sewage sludge in agriculture in Romania*, Materiale Plastice, vol. 55, nr. 4, p. 700-703, 2018.

[5]. Zanoschi V., Toma C., *Morphology and anatomy of cultivated plants*, Ed. Ceres, Bucharest, (In Romanian), 1985.

[6]. Gomes S. M. S., Lima V. L. A., Souza A. P., Nascimento J. J. V. R., Nascimento E., *Cloroplast pigments as indicators of lead stress*, Engenharia Agrícola, Jaboticabal, 34, p. 877-884. 2014.

[7]. Lichtenthaler H., Buschmann C., *Chlorophylls and Carotenoids. Measurement and Characterization by UV-Vis Spectroscopy*, Current Protocols in Food Analytical Chemistry, F4: 3.1-3.8, 2001.

[8]. Gang P., Xiu-Lan X., Qian J., Song S., Chang-Jie X., *Chlorophyll a/b binding protein plays a key role in natural and ethylene-induced degreening of Ponkan (Citrus reticulata Blanco)*, Scientia Horticulturae, 160, p. 37-43, 2013.

[9]. Ritchie R., *Consistent sets of spectrophotometric chlorophyll equations for acetone, methanol and ethanol solvents*, Photosynthesis Research, 89, p. 27-41, 2006.

[10]. Ritchie R., *Universal chlorophyll equations for estimating chlorophylls a, b, c, and d and total chlorophylls in natural assemblages of photosynthetic organisms using acetone, methanol, or ethanol*, Photosynthetica, 46, p. 115-126, 2008.

[11]. C. I. E., *Technical Report: Colorimetry*, 3rd ed., Publication 15, Central Bureau of the CIE, Vienna, 2004.

[12]. Krystian M., Stanislaw L., *Chlorophyll extraction from leaves, needles and microalgae: A kinetic approach*, International J. of Agricultural and Biological Eng., 6, p. 107-115, 2013.

[13]. Qingjie D., Dalong Z., Xiaocong J., Xiaoming S., Jianming L., *Effects of atmospheric and soil water status on photosynthesis and growth in tomato*, Plant, Soil and Env., 64, p. 13-19. 2018.

[14]. Goncalves J. F. C., Marenco R. A., Vieira G., *Concentration of photosynthetic pigments and chlorophyll fluorescence of mahogany and tonka bean under two light environments*, Braz. J. of Plant Physiology, 13, p. 149-157, 2001.

[15]. Poongodi N., Sasikala T., *Effect of detergent on selected morphological and biochemical parameters of green gram (Vigna radiata L.)*, Biotechnology, 2(7), p. 9-10, 2013.

[16]. Cretu R., Circiumaru A., Murariu G., *Effect of Liquid Detergents on the Biochemical Parameters of Some Plantlets*, Materiale Plastice, 55, 4, p. 575-579, 2018.

MANUSCRISELE, CĂRŢILE ŞI REVISTELE PENTRU SCHIMB, PRECUM ŞI ORICE CORESPONDENŢE SE VOR TRIMITE PE ADRESA:

MANUSCRIPTS, REVIEWS AND BOOKS FOR EXCHANGE COOPERATION, AS WELL AS ANY CORRESPONDANCE WILL BE MAILED TO:

LES MANUSCRIPTS, LES REVUES ET LES LIVRES POUR L'ECHANGE, TOUT AUSSI QUE LA CORRESPONDANCE SERONT ENVOYES A L'ADRESSE:

MANUSCKRIPTEN, ZIETSCHRITFTEN UND BUCHER FUR AUSTAUCH SOWIE DIE KORRESPONDENZ SID AN FOLGENDE ANSCHRIFT ZU SEDEN:

After the latest evaluation of the journals by the National Center for Science Policy and Scientometrics (**CENAPOSS**), in recognition of its quality and impact at national level, the journal will be included in the B^+ category, 215 code (http://cncsis.gov.ro/userfiles/file/CENAPOSS/Bplus_2011.pdf).

The journal is already indexed in:

SCIPIO-RO: http://www.scipio.ro/web/182206

EBSCO: http://www.ebscohost.com/titleLists/a9h-journals.pdf

Google Academic: https://scholar.google.ro

Index Copernicus: https://journals.indexcopernicus.com

The papers published in this journal can be viewed on the website of "Dunarea de Jos" University of Galati, the Faculty of Engineering, pages: http://www.sim.ugal.ro, http://www.imsi.ugal.ro/Annals.html.

Name and Address of Publisher:
Contact person: Elena MEREUȚĂ
Galati University Press - GUP
47 Domneasca St., 800008 - Galati, Romania
Phone: +40 336 130139
Fax: +40 236 461353
Email: gup@ugal.ro

Name and Address of Editor:
Prof. Dr. Eng. Marian BORDEI
"Dunarea de Jos" University of Galati, Faculty of Engineering
111 Domneasca St., 800201 - Galati, Romania
Phone: +40 336 130208
Phone/Fax: +40 336 130283
Email: mbordei@ugal.ro

AFFILIATED WITH:

- THE ROMANIAN SOCIETY FOR METALLURGY
- THE ROMANIAN SOCIETY FOR CHEMISTRY
- THE ROMANIAN SOCIETY FOR BIOMATERIALS
- THE ROMANIAN TECHNICAL FOUNDRY SOCIETY
- THE MATERIALS INFORMATION SOCIETY (ASM INTERNATIONAL)

Edited under the care of the FACULTY OF ENGINEERING

Annual subscription (4 issues per year)

Fascicle DOI: https://doi.org/10.35219/mms

Volume DOI: https://doi.org/10.35219/mms.2019.3

Editing date: 15.09.2019
Number of issues: 200
Printed by Galati University Press (accredited by CNCSIS)
47 Domneasca Street, 800008, Galati, Romania